Ensemble-Based Error and Predictability Metrics Associated with Tropical Cyclogenesis. Part II: Wave-Relative Framework

WILLIAM A. KOMAROMI

National Research Council, Monterey, California

SHARANYA J. MAJUMDAR

Rosenstiel School of Marine and Atmospheric Science, University of Miami, Miami, Florida

(Manuscript received 4 September 2014, in final form 2 January 2015)

ABSTRACT

The predictability of selected variables associated with tropical cyclogenesis is examined using 10-day ECMWF ensemble forecasts for 21 events from the 2010 Atlantic hurricane season. Variables are associated with the strength of the pregenesis disturbance, quantified via circulation and thickness anomaly, and the favorability of the immediate environment via moisture and vertical wind shear.

For approximately half of the cases, the predicted strength of the genesis signal is directly related to the predicted favorability of the environment. For the remainder of the cases, predictability is more directly associated with the strength and location of the analyzed disturbance. Some commonalities among the majority of the sample are also observed. Forecast joint distributions demonstrate that 700-hPa relative humidity of less than 60% within 300 km of the circulation center is a limiting factor for genesis. Genesis is also predicted and found to occur in the presence of significant wind shear ($\sim$15 m s^{-1}), but almost exclusively when the core and environment of the wave are both very moist.

The ensemble also demonstrates the potential to predict error standard deviation of variables averaged within 300- and 1000-km radii about individual tropical waves. Forecasts with greater ensemble standard deviation tend to be, on average, associated with greater mean error, especially for forecasts of less than 7 days. However, model biases, particularly a dry core and weak circulation bias, become pronounced at longer lead times. Overall, these results demonstrate that both the environmental conditions favorable to genesis and the genesis events themselves may be predictable to a week or more.

1. Introduction

Tropical cyclone formation (hereafter referred to as "genesis") depends upon both the favorability of the large-scale environment and the cooperation of smaller-scale processes. During each season, there are active periods that produce multiple tropical cyclones, while other periods are inactive. In parallel, the predictability of genesis is expected to depend on the predictability of relevant processes on all scales. To investigate this, Komaromi and Majumdar (2014, hereafter Part I), quantified the predictability and predictive skill of atmospheric variables over a large fixed area spanning the Atlantic basin, using the Ensemble Prediction System from the European Centre for Medium-Range Weather Forecasts (ECMWF). The variables included those used to identify tropical waves and cyclones (e.g., lower-tropospheric circulation and local thickness anomaly), and environmental variables (e.g., vertical wind shear and relative humidity). Several metrics were explored, including growth and saturation of error, predicted forecast error standard deviation, and predictive power. In Part I, the variables that were more directly related to large-scale phenomena were found to possess a longer time range of predictability than those related to small-scale processes. Additionally, daily and monthly variations in predictability were evident, and were dependent on the flow regime. The potential for the ensemble to predict the standard deviation of the variables in 10° × 10° boxes across the basin was demonstrated. While these

Corresponding author address: William A. Komaromi, Naval Research Laboratory, 7 Grace Hopper Ave., Monterey, CA 93943. E-mail: william.komaromi.ctr@nrlmry.navy.mil

DOI: 10.1175/MWR-D-14-00286.1

results conveyed the predictability concepts on a basin-wide scale, the predictability of genesis itself needs to be assessed locally with respect to the wave that develops into the cyclone. In this paper (Part II), we narrow the focus to explore predictability in a moving frame of reference centered on the developing wave.

A few studies that investigate the predictability associated with individual tropical disturbances prior to genesis have been published. First, Sippel and Zhang (2008) used a mesoscale ensemble to investigate the predictability of a nondeveloping tropical wave. They found that the genesis in some ensemble members was sensitive to the availability of high CAPE and sufficient deep-layer moisture. Based on this result, they suggested that genesis requires sustained convection in the presence of a sufficiently moist environment, which limits the detrimental effects of dry downdrafts. A similar study by Sippel et al. (2011) found the genesis of Tropical Storm Debby (2006) to be sensitive to nearby dry air associated with a Saharan air layer (SAL) outbreak, with the strongest vortex in the moistest members. Quite notably, the sensitivity to the dry environment depended considerably on cyclone strength, and it became insignificant once a tropical storm formed. Sensitivity to secondary detrimental effects, including warm temperatures within the SAL and shear associated with the African easterly jet, was also observed. More recently, the problem has been investigated using data from the National Science Foundation's Pre-Depression Investigation of Cloud-Systems in the Tropics (PREDICT) field campaign in 2010 (Montgomery et al. 2012). Observational studies found genesis to be associated with greater midlevel moisture but not necessarily associated with greater CAPE (Smith and Montgomery 2012; Komaromi 2013).

As already alluded to, predictability of tropical cyclone formation is often limited by uncertainty in the initial conditions. A number of studies have examined the sensitivity to perturbed initial conditions in the vicinity of the tropical cyclone and/or pregenesis disturbance by using an ensemble Kalman filter (EnKF), singular vectors (SVs), or ensemble-based or adjoint-based sensitivity. Most of these singular vector studies tend to focus more on perturbation magnitude and growth in the wind field in a box surrounding the TC, and this tends to be dominated by errors in track. However, a few studies that focus on formation do exist. Using an EnKF ensemble, Torn and Cook (2013) found that the initial-condition sensitivity of two developing tropical cyclones differed considerably. For the genesis of Danielle (2010), the magnitude of the circulation was found to be most sensitive to the strength of the upper-level divergence and the vertical wind shear. For Karl (2010), the circulation was found to be most sensitive to the strength of the initial vortex. Again using mesoscale ensembles and an EnKF, Poterjoy and Zhang (2014) found that the assimilation of PREDICT dropwindsonde data increased the strength of the low- to midlevel circulation, moistened the column, and decreased position errors of the initial vortex that developed into Karl (2010). Last, an adjoint sensitivity study by Doyle et al. (2012) found TC intensity to be very sensitive to perturbations in the moisture and temperature fields, with the most efficient intensification occurring when moistening occurs in the lower and middle levels and when heating occurs in banded regions of maximum relative vorticity in the initial state. Optimal adjoint perturbations exhibited rapid growth for the developing TC and only modest growth for the nondeveloping system. These studies all suggest that uncertainty on the mesoscale limits the predictability of genesis. Last, the ability of deterministic global models to predict genesis was examined by Halperin et al. (2013), and a probabilistic verification of genesis in global and mesoscale ensembles was conducted by Majumdar and Torn (2014). Both these studies demonstrated some promise in genesis prediction and identified some deficiencies in the models.

In this study, we use the same 10-day ECMWF ensemble predictions employed in Part I for a sample of 21 genesis cases in the Atlantic basin in 2010 to ask the following questions in the wave-relative framework. (i) From storm to storm, how does the nature of the predictability of relevant variables valid at the genesis time evolve with forecast time, and are the results consistent across the cases? (ii) Over the season, are forecasts of pairs of relevant variables and their errors correlated? (iii) Is the ensemble capable of predicting forecast error variance, and does it compare favorably with the results in the large-scale framework of Part I? The questions are addressed in the context of the main local fields relevant to genesis (e.g., relative humidity, wind shear), and their effects on quantities that characterize the strength (e.g., circulation). The methodology and metrics used are described in section 2, followed by four individual case examples in section 3 to address question (i). In section 4, joint forecast distributions accumulated over the season are presented to address question (ii), and question (iii) on variance prediction is examined in section 5. Conclusions follow in section 6.

2. Methodology

a. *ECMWF ensemble and cases*

As in Part I, analyses and 10-day forecasts from the operational 50-member ECMWF Ensemble Prediction System at T639 L62 resolution, interpolated onto

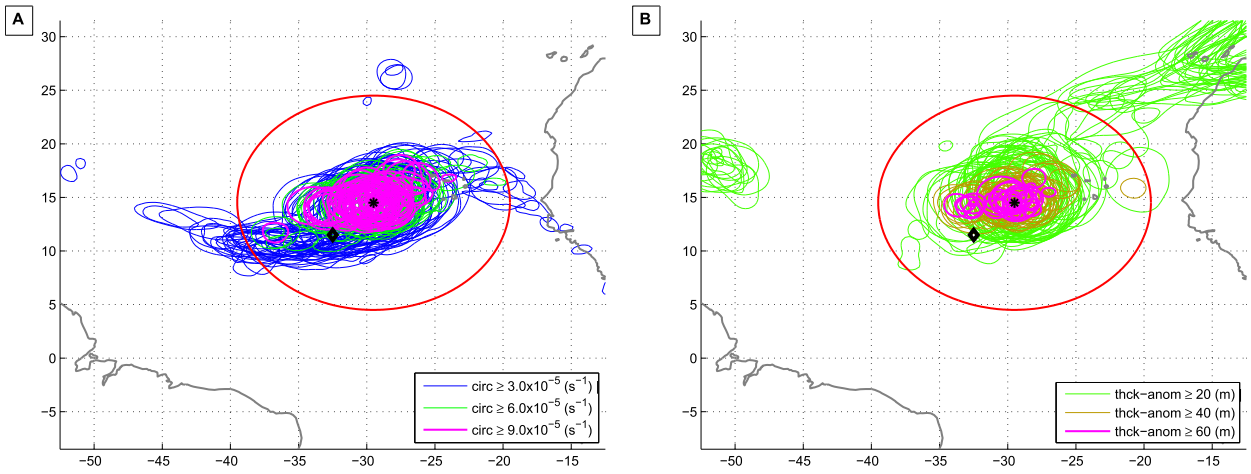

FIG. 1. Depiction of the search algorithm, with (a) circulation contours and (b) thickness anomaly contours. Centers of maximum circulation and local maxima in thickness anomaly are found within 1000-km radius (red circle) of the maximum ensemble mean circulation (black star). The maximum ensemble mean circulation is allowed to vary up to 1000 km from the verifying point of genesis (black diamond).

a horizontal grid with 0.25° spacing are used. The ensemble data, produced at 0000 and 1200 UTC each day, were provided via the THORPEX Interactive Grand Global Ensemble (TIGGE) database (Bougeault et al. 2010, http://tigge.ecmwf.int/). Further details of the ensemble construction are given in Part I. The time of genesis is defined as the first declaration of a tropical depression or tropical storm in the National Hurricane Center (NHC) best track. Genesis events that occur between ECMWF analysis times are assigned to the next available ECMWF analysis.

A total of 21 tropical cyclones formed in the Atlantic basin during 2010. Of these, 15 were related to African easterly waves, either developing directly from African easterly waves (e.g., Danielle, Earl, Fiona, Igor, and Julia) or from a wave that was interacting with another system such as a low pressure area (e.g., Bonnie and Karl).

b. *Variables in wave-relative framework*

As in Part I, the following variables are used for each ensemble member:

(i) relative vorticity: 850 hPa;
(ii) vertical shear of horizontal wind: 850–200 and 850–500 hPa;
(iii) divergence: 200 and 850 hPa;
(iv) relative humidity (RH): 700 hPa;
(v) circulation: average 850–700-hPa relative vorticity within 200 km of each grid point; and
(vi) thickness anomaly, defined by

$$\Delta Z = Z_{r=100\,\mathrm{km}} - Z_{r=1000\,\mathrm{km}}. \qquad (1)$$

The mean of each of the aforementioned variables is then computed over a 0–300-km radius "core" and a 300–1000-km radius "environment" about the center of the tropical wave in each ensemble member at each lead time. In contrast to Part I, velocity potential is not computed here. This is because variations in velocity potential tend to occur on larger scales than individual tropical waves, and it is therefore more appropriate for large-scale diagnostics.

The procedure for determining the center of the tropical wave is as follows. First, circulation is calculated at each grid point using a 200-km radius in each ensemble member at all lead times. This radius was chosen for consistency with Komaromi and Majumdar (2014) and Majumdar and Torn (2014). Since ensemble forecasts may have a significant position bias, particularly at large lead times, the location of the tropical wave in the model is chosen to be the location of the greatest ensemble-mean circulation (e.g., black star in Fig. 1) within a 1000-km radius (red circle) of the verifying genesis location (black diamond). Centers of circulation are then determined from each individual ensemble member as the location of maximum circulation within 1000 km of the maximum ensemble mean circulation (Fig. 1a). All locations of the maximum thickness anomaly within 1000 km of the center of the maximum ensemble mean circulation are also located (Fig. 1b). The working center is then taken to be an average of the positions determined via the circulation and thickness anomaly. The two respective centers in each ensemble member are found to differ rarely (~1% of the time) by more than 100 km.

Although the circulation in the ECMWF analysis at the onset of genesis differs from case to case, values exceeding $9 \times 10^{-5}\,s^{-1}$ normally correspond to cases in which genesis has occurred [assuming a sufficient warm core and minimum sea level pressure, see Majumdar and Torn (2014) for details]. In Fig. 1 and in section 3a, the ensemble members with values of circulation exceeding this value are color coded in magenta. Lower circulation values between 6–9 $\times$ 10^{-5} and 3–6 $\times$ $10^{-5}\,s^{-1}$ and $<3 \times 10^{-5}\,s^{-1}$ are color coded in green, blue, and black, respectively.

c. Joint distributions

Two-dimensional (and occasionally three dimensional) joint distributions over the full sample of cases are examined to determine the relationship, if any, between the variables and their errors over all ensemble forecasts leading up to the genesis time. These joint distributions are normalized by the number of entries in each column to account for the unequal distribution of samples within a larger array of possible environments. Because of this normalization, the integral of each column is equal to 1. Thus, they are similar to, but not equivalent to, marginal distributions, in which the entire joint distribution is normalized by the total number of points in all rows and columns and, therefore, the integral over the entire distribution is equal to 1. In section 4, joint distributions between variables, joint distributions of errors in these variables, and lagged joint distributions are all presented. Joint distributions of error are a simple way of examining the relationship between the forecast errors of one variable with the forecast errors of another, and are expected to depict the same physical relationships as seen in the variables themselves. Last, lagged joint distributions relate the values of one variable "A" 24 and 48 h before genesis with the value of another variable "B" at the time of genesis. By computing lagged A versus B and comparing it to A versus lagged B, it is often possible to separate the effect of A on B versus B on A.

d. Variance prediction

Ensemble forecasts offer additional information over a single deterministic forecast by offering a forecast distribution or PDF. The most basic higher moment is the ensemble variance, which serves as a prediction of the forecast error variance σ^2_{M-1}:

$$\sigma^2_{M-1}(t) = \frac{1}{M-1}\sum_{i=1}^{M}[x_i^f(t) - \overline{x^f(t)}]^2, \qquad (2)$$

where M is the total number of ensemble members (50 members plus 1 control run here), and $\overline{x^f(t)}$ is the ensemble mean forecast of x at time t. There has been considerable debate about how to evaluate the reliability of ensemble predictions via their statistical consistency versus actual errors. The ensemble needs to be able to discriminate between different error distributions, with forecasts of higher error corresponding to larger error spread in the ensemble predictions. If the ensemble is well constructed, then the variance of solutions in individual ensemble members should reflect the actual uncertainty in the forecast (Wang and Bishop 2003). In other words, a PDF of predicted forecast errors should closely resemble the PDF of actual forecast errors (DelSole 2004). To quantify this, one approach is to determine whether a relationship exists between the predicted error variance [Eq. (2), or the standard deviation, which is its square root] and the corresponding variance (or standard deviation) of actual errors in the ensemble mean, given by

$$\frac{1}{B-1}\sum_{b=1}^{B}[\overline{x_b^f(t)} - x_b^a(t)]^2 \qquad (3)$$

for the bth forecast in variance bin of size B. This is accomplished by first plotting the distribution of forecast errors of the ensemble mean versus their corresponding predictions of the standard deviation of the ensemble mean, for each forecast case. Then, by averaging the data points in equally sized bins of increasing predicted forecast error variance, the standard deviation of the actual errors is computed for each bin, analogous to Majumdar et al. (2001). Ideally, a linear, increasing relationship of slope 1 between the predicted and actual error standard deviation is found.

The ability of the ensemble forecasts to predict uncertainty is evaluated in section 5, using the same methodology as Part I, though for a disk of radius 300 km (core) and an annulus of radius 300–1000 km (environment) centered on the tropical wave. Following Grimit and Mass (2007), we plot the root-mean-square (RMS) error of the ensemble mean relative to the verifying control analysis, retaining the sign of the errors, versus the standard deviation of the ensemble forecast. In this way, the distribution of forecast errors, including any biases and departures from Gaussianity, are illustrated, while retaining the ability to formally evaluate the relationship between the predicted and actual error range. While the traditional approach is to examine error growth from a fixed initialization time out to some time at which error is maximized, this study will instead fix the verification time and allow initializations and subsequent forecasts verifying at this time to vary. Therefore, time of initialization will flow chronologically from left to right, while forecast time and

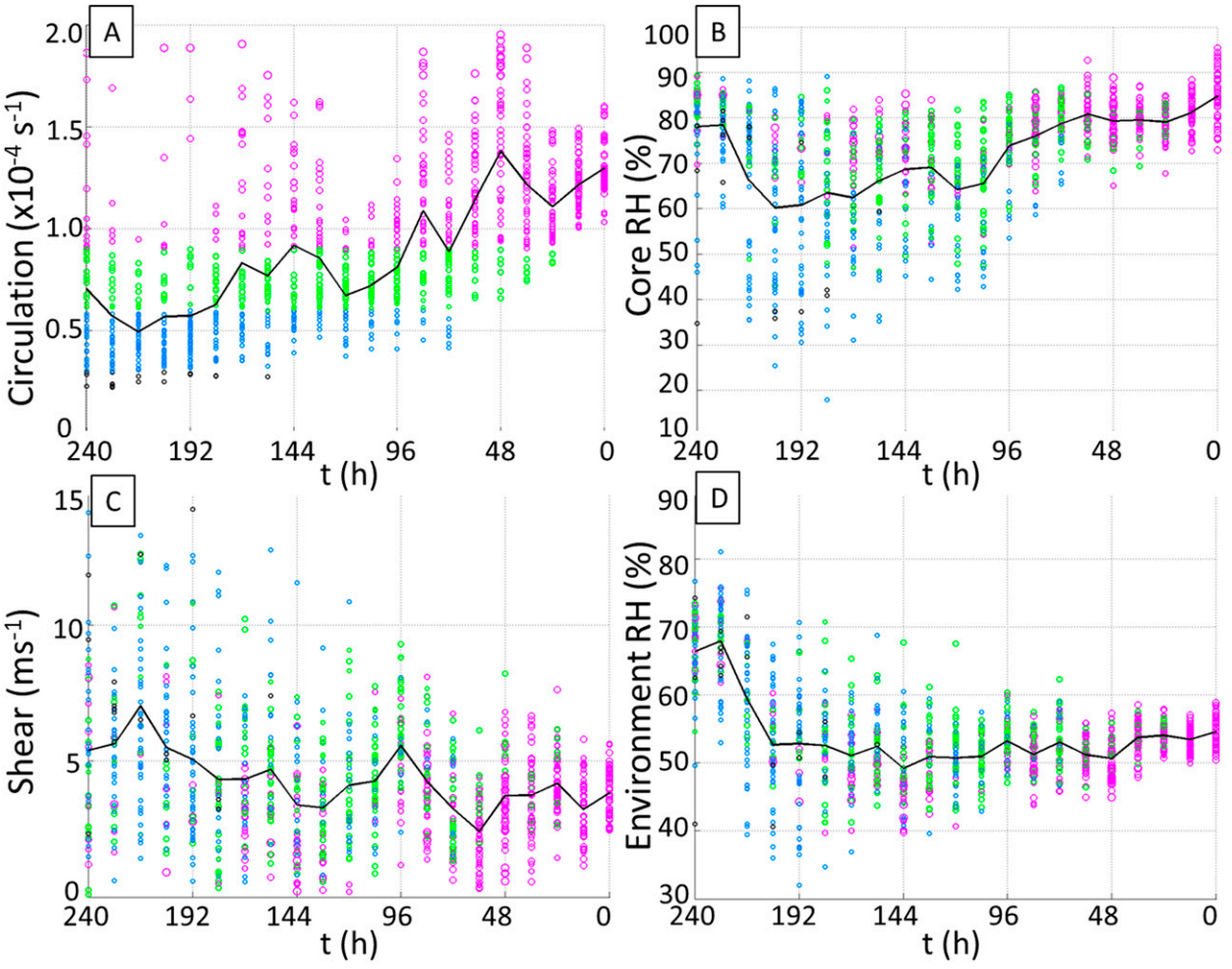

FIG. 2. Ensemble forecast distributions as a function of lead time (h, x axis) valid at the time of genesis (1200 UTC 25 Aug 2010) for Hurricane Earl, with (a) circulation (s^{-1}), (b) core RH (%) at 700 hPa, (c) environmental 850–200-hPa wind shear ($m\,s^{-1}$), and (d) environmental RH (%) at 700 hPa. Each dot represents a different ensemble member with forecast circulation values of $<3 \times 10^{-5}\,s^{-1}$ (black), $\geq 3 \times 10^{-5}\,s^{-1}$ (blue), $\geq 6 \times 10^{-5}\,s^{-1}$ (green), and $\geq 9 \times 10^{-5}\,s^{-1}$ (magenta). The ensemble mean forecast is also shown (black line).

subsequent error will increase from right to left. The data points plotted are for all 21 genesis cases.

Last, the predictive power (Schneider and Griffies 1999) that was utilized in Part I is not used in the wave-relative framework. This is because it is difficult to define a climatological error covariance matrix that is directly comparable to the ensemble forecast error covariance matrix. A 10-day forecast error covariance matrix might include everything ranging from dissipation in the weakest ensemble members to a borderline hurricane in the strongest ensemble members. In comparison, a climatological error covariance that only includes verifying genesis events would have too narrow a distribution of potential outcomes, and, therefore, too low an error covariance. Alternatively, a climatological error covariance that includes all waves and TCs has too broad a distribution. Ultimately, the results proved to be too sensitive to the subjective nature of defining these upper and lower cutoff thresholds from which the climatological distribution is calculated.

3. Ensemble predictions for individual cases

a. Earl

The first genesis event examined is Earl (2010), in which the relationship between the favorability of the forecast environment and the forecast strength of circulation valid at the time of genesis is fairly straightforward. Even at 240 h, many ensemble members valid at the time of genesis show a circulation of at least moderate strength ($6 \times 10^{-5}\,s^{-1}$) within the verifying genesis region (Fig. 2a). With the exception of an occasional drop-off in strength of circulation that occurs at

120 h, the strength of the ensemble-mean circulation (solid black line) increases steadily from long-range forecasts to short-range forecasts, through to genesis at $t = 0$ h. However, at 120 h, the verification (the ensemble mean at $t = 0$ h) falls outside the entire ensemble, suggesting an inability of the ensemble at this time to capture the appropriate circulation. As expected, the number of ensemble members indicating very weak (black), weak (blue), or moderate (green) circulations decreases while the number of members indicating a stronger (magenta) circulation increases as the initial time approaches the genesis time. With a verification of $1.27 \times 10^{-4}\,s^{-1}$ at $t = 0$ h in the ensemble mean, Earl was associated with a particularly strong circulation at the time of genesis, likely due at least in part to the large size of the tropical wave from which it formed.

The next step is to examine the evolution of the forecasts of environmental wind shear, core RH, and environmental RH, with the ensemble members color coded by strength of circulation. While there is good agreement very early on among ensemble members that 850–200-hPa environmental wind shear will be low ($<10\,m\,s^{-1}$) and 700-hPa core RH will be high, a few outliers predicting a high shear environment or dry core do exist more than 96 h before genesis (Figs. 2b,c). Also note in Fig. 2c that at any particular forecast lead time, the ensemble members that possess the lowest shear often possess the strongest circulation (strongest members represented by magenta dots), while the members with the greatest shear are often associated with the weakest circulation (weakest members in black/blue). Similarly, the strongest (weakest) members at any particular lead time are often associated with the greatest (lowest) core RH (Fig. 2b). This suggested sensitivity of vortex strength to midlevel RH close to the circulation of the developing TC corroborates well with the findings of Doyle et al. (2012). Despite a clear positive relationship between core moisture and strength of circulation, a near-opposite relationship between environmental moisture and strength of circulation is found (Fig. 2d). This apparent paradox is due to the fact that the ensemble members that strengthened the circulation more quickly produced a solution in which the wave began to gain latitude more rapidly. This gain in latitude is possibly a consequence of "beta drift," in which the northwestward drift of a vortex due to the development of beta gyres that form via the advection of planetary vorticity by the storm-scale cyclonic circulation is proportional to the strength of the vortex circulation (Fiorino and Elsberry 1989).

In addition to the aforementioned contrast between core RH (Fig. 2b) and environmental RH (Fig. 2d), there is also a stark difference in magnitudes. While core RH is between 80% and 90%, environmental RH is between 50% and 60%. This is also the case for several other easterly waves during 2010. Occasionally, the easterly wave becomes cut off from a larger moisture source (often to the south) as the wave penetrates deep into a large air mass of less humid air (Fig. 3a). Even though the environment can be relatively dry, an insignificant amount of less humid air actually penetrates the core and the system still develops. This limited penetration of relatively dry environmental air appears to be especially common for larger circulations associated with larger regions of core moisture. This finding is consistent with the "marsupial paradigm," in which a recirculating region of moisture collocated with the critical layer of the predepression avoids interaction with the drier environmental air located outside the critical layer (Dunkerton et al. 2009). Observations (Braun et al. 2013) and idealized simulations (Braun et al. 2012) also suggest that dry air >300 km from the storm center does not enter the recirculating region. However, these ideas have only been developed for cases in which shear is low, of which Earl is also a case. The applicability of the marsupial paradigm and whether or not the system can avoid interaction with a dry environment in a more sheared regime has not been explored. Fiona, which will be discussed in greater detail next, is another case in which a pocket of higher RH become detached from a broader environment of high RH farther southeast (Fig. 3b).

Another important concept illustrated by Earl is the relationship between uncertainty in the environment and how this translates to uncertainty in the strength of circulation at the time of genesis. More specifically, sharp gradients in environmental shear or moisture are often associated with increased forecast variance due to greater uncertainty as to where that gradient will be located. When a tropical wave such as Earl is projected to be located along a gradient in moisture, some circulations ingest a significant amount of dry air (red stars) while others do not (green stars; Fig. 3c). The result is large variance in the environmental moisture, such as in the 168-h forecast (Fig. 2b). While the exact pathway from environmental moisture variance to variance in circulation is not fully explored, a correlation between the two is certainly evident for Earl, suggesting a causal relationship between uncertainty in the environment and uncertainty in the strength of the predicted circulation (Fig. 2a). On the other hand, once the ensemble reaches an agreement as to which side of the moisture (or shear) gradient the wave will be located (Fig. 3d), the variance in the moisture forecast drops considerably. This ultimately contributes to a reduction in the variance in the circulation forecast (Fig. 2a). Therefore, there is a clear link between the uncertainty in the strength of circulation and the uncertainty in the

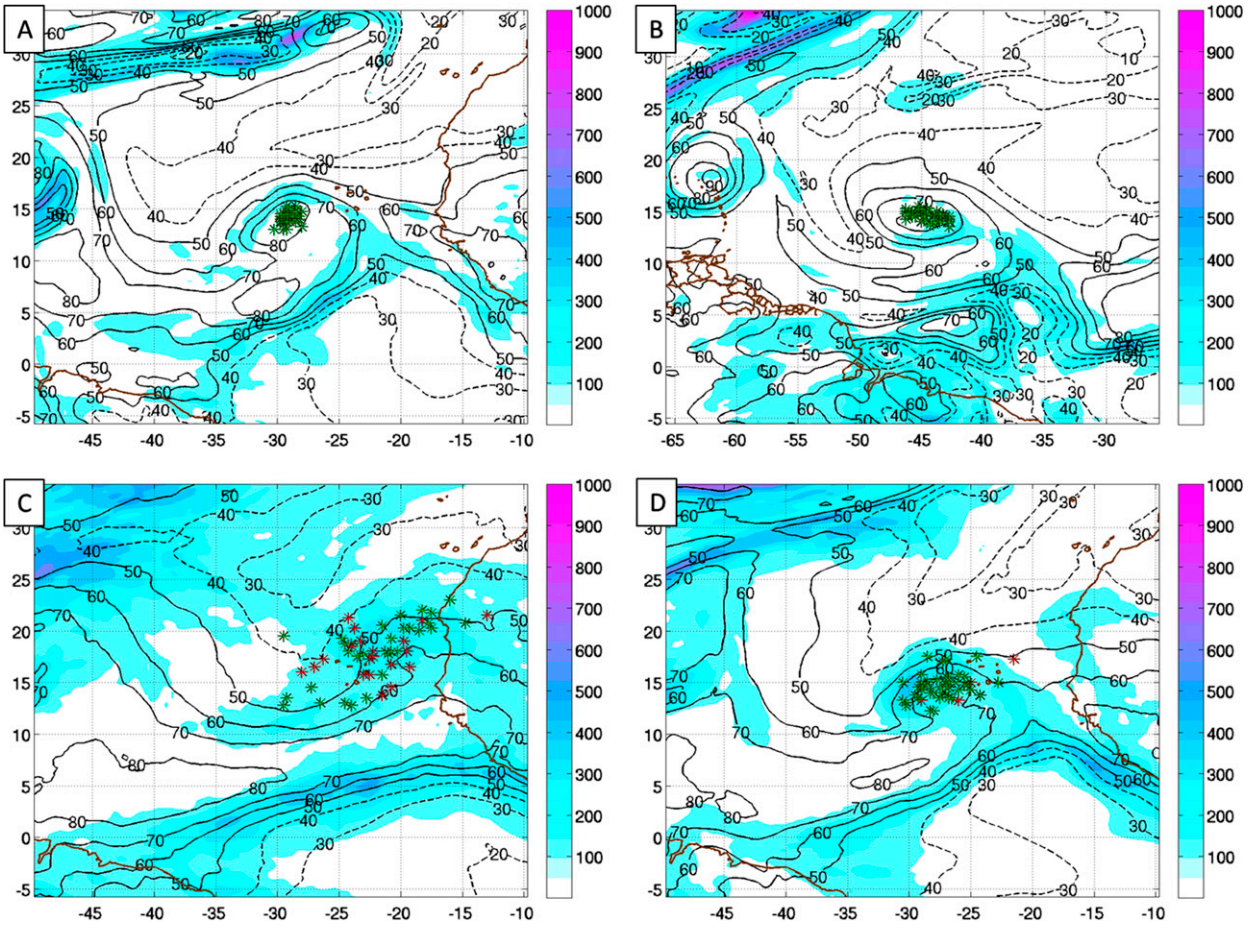

FIG. 3. Ensemble mean RH at 700 hPa (contours), forecast variance for RH (color shaded), and centers of circulation with moist (700-hPa RH $\geq$ 60%; green asterisks) and dry (700-hPa RH $<$ 60%; red asterisks) cores in each ensemble member. Included are (a) a 24-h forecast valid at the time of genesis of Earl from 1200 UTC 24 Aug 2010, (b) a 24-h forecast valid at the time of genesis of Fiona from 1200 UTC 29 Aug 2010, (c) a 168-h forecast for Earl from 1200 UTC 18 Aug 2010, and (d) a 96-h forecast for Earl from 0000 UTC 21 Aug 2010.

location of the wave and/or location of gradients of environmental variables.

b. *Fiona*

In addition to being a case with a moist core embedded in a relatively dry environment, Fiona was interesting in that there was virtually no genesis signal in the ensemble between 144 and 240 h prior to genesis, followed by a rapid transition toward a strong signal for genesis from the 96–120-h lead time (Fig. 4a). In fact, the ensemble over-adjusted as the predicted strength of circulation was too strong in most members from the 48–96-h lead time. For lead times of 96 h and shorter, fewer ensemble members predict a dry core (Fig. 4b), a dry environment (not shown), or a high shear environment (Fig. 4c) as an increasing number of members simultaneously produce a stronger circulation. We, therefore, suggest that a more accurate forecast of the environmental parameters contributes to a superior genesis forecast at these shorter lead times. Additionally, within the 96–132-h time frame, individual members with the strongest circulation (magenta dots) are generally of higher core RH while members with the weakest circulation (blue/green dots) are of lower core RH. This demonstrates that a buildup of inner core moisture is essential to building a stronger circulation for Fiona at these lead times.

While changes in predicted environmental conditions likely contributed somewhat to changes in predicted strength of circulation, they were likely too subtle to be the only factor. Interestingly, 108 h prior to the genesis of Fiona also corresponds to the timing in which the pre-Fiona wave first emerged into the Atlantic from the coast of Africa (Fig. 4d). As upper-air data are particularly sparse over Africa, the vortex was likely poorly initialized in many successive model runs. In addition to being better initialized with data from radiosondes launched from Dakar, Senegal, as the wave passed over it, it is also possible that the initialization of the ECMWF

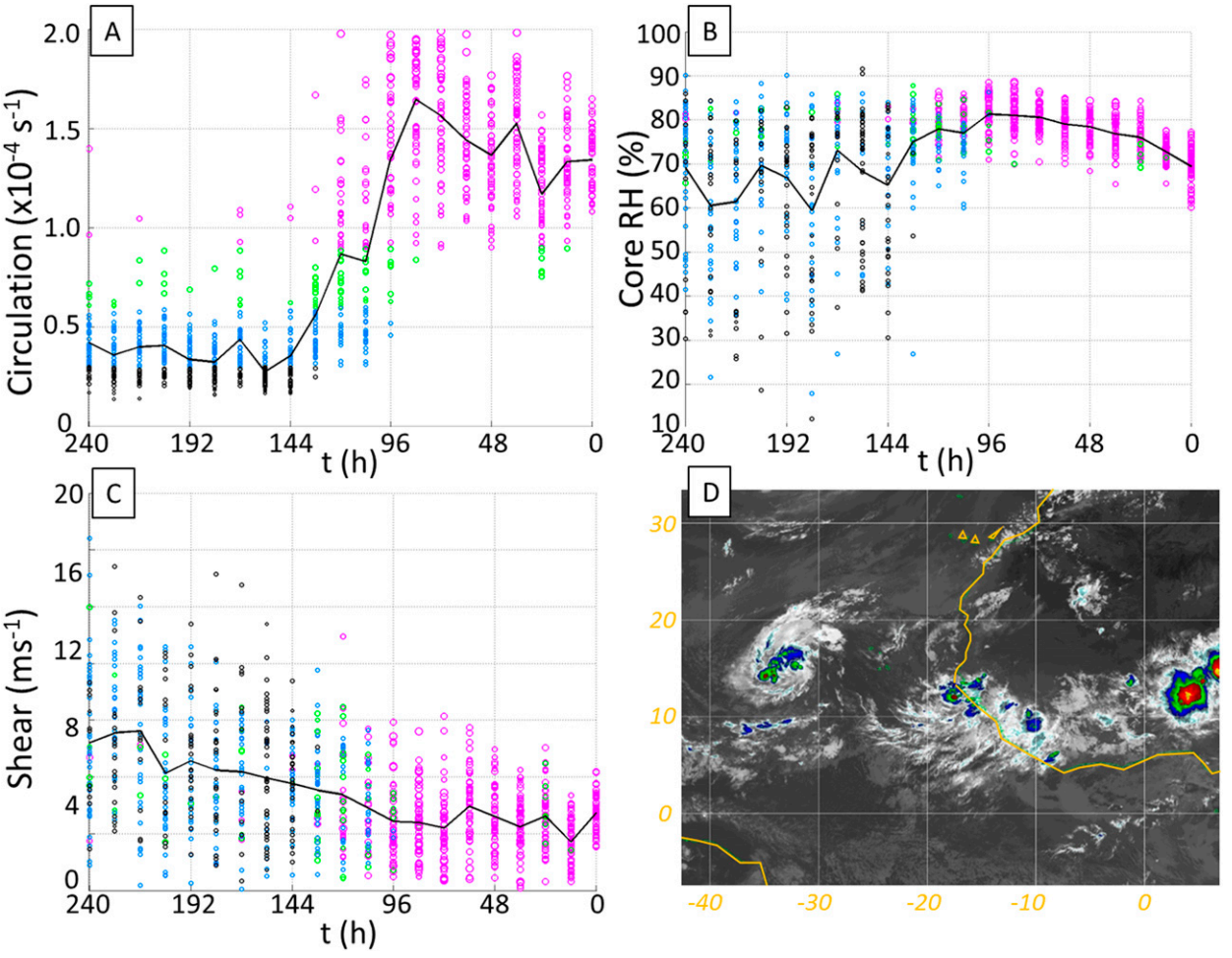

FIG. 4. Ensemble forecast distributions as a function of lead time (h, *x* axis) valid at the time of genesis (1200 UTC 30 Aug 2010) for Tropical Storm Fiona, with (a) circulation (s^{-1}), (b) core RH (%) at 700 hPa, (c) environmental 850–200-hPa wind shear ($m\,s^{-1}$), and (d) a *GOES-12* and *EUMETSAT-8* composite infrared satellite image of the easterly wave that spawns Fiona exiting the west coast of Africa 108 h prior to genesis (0000 UTC 26 Aug 2010; http://catalog.eol.ucar.edu/predict/). In (a)–(c), each dot represents a different ensemble member with forecast circulation values of $<3 \times 10^{-5}\,s^{-1}$ (black), $\geq 3 \times 10^{-5}\,s^{-1}$ (blue), $\geq 6 \times 10^{-5}\,s^{-1}$ (green), and $\geq 9 \times 10^{-5}\,s^{-1}$ (magenta). The ensemble mean forecast is also shown (black line).

ensemble improved once the wave emerged over water as data retrieved via microwave profiles such as total precipitable water are not available over land. For these reasons, it appears as though the predictive skill of genesis for Fiona is directly related to whether the parent wave is over Africa or not at the time of model initialization. While Fiona was perhaps the most obvious case, other genesis events such as Lisa and Tomas (to a lesser degree) appear to have been associated with decreased predictive skill while their pregenesis disturbances were located over Africa.

c. *Igor*

The genesis of Igor occurred in an environment of unusually high shear, with 850–200-hPa shear exceeding $14\,m\,s^{-1}$ (Fig. 5c). This was the greatest value of shear to be associated with any genesis event in 2010. Meanwhile, Igor was also associated with one of the strongest circulation values at the time of genesis (Fig. 5a) and was a rare case in that the strength of predicted shear generally increased with decreasing lead time before genesis. While forecasts for higher values of environmental shear often prevent particular ensemble members from predicting genesis for most other events in 2010, Igor appears to be a case where a large and strong initial circulation was able to overcome stronger shear. The strength of the predicted circulation at the time of genesis from Igor appears to have been strongly related to the strength of the circulation 48 h prior to genesis in the 120- and 168-h forecasts. A moderate-strength vortex (in most ensemble members) exiting the African coast resulted in a moderate-to-strong vortex at the time of genesis (not shown). At shorter lead

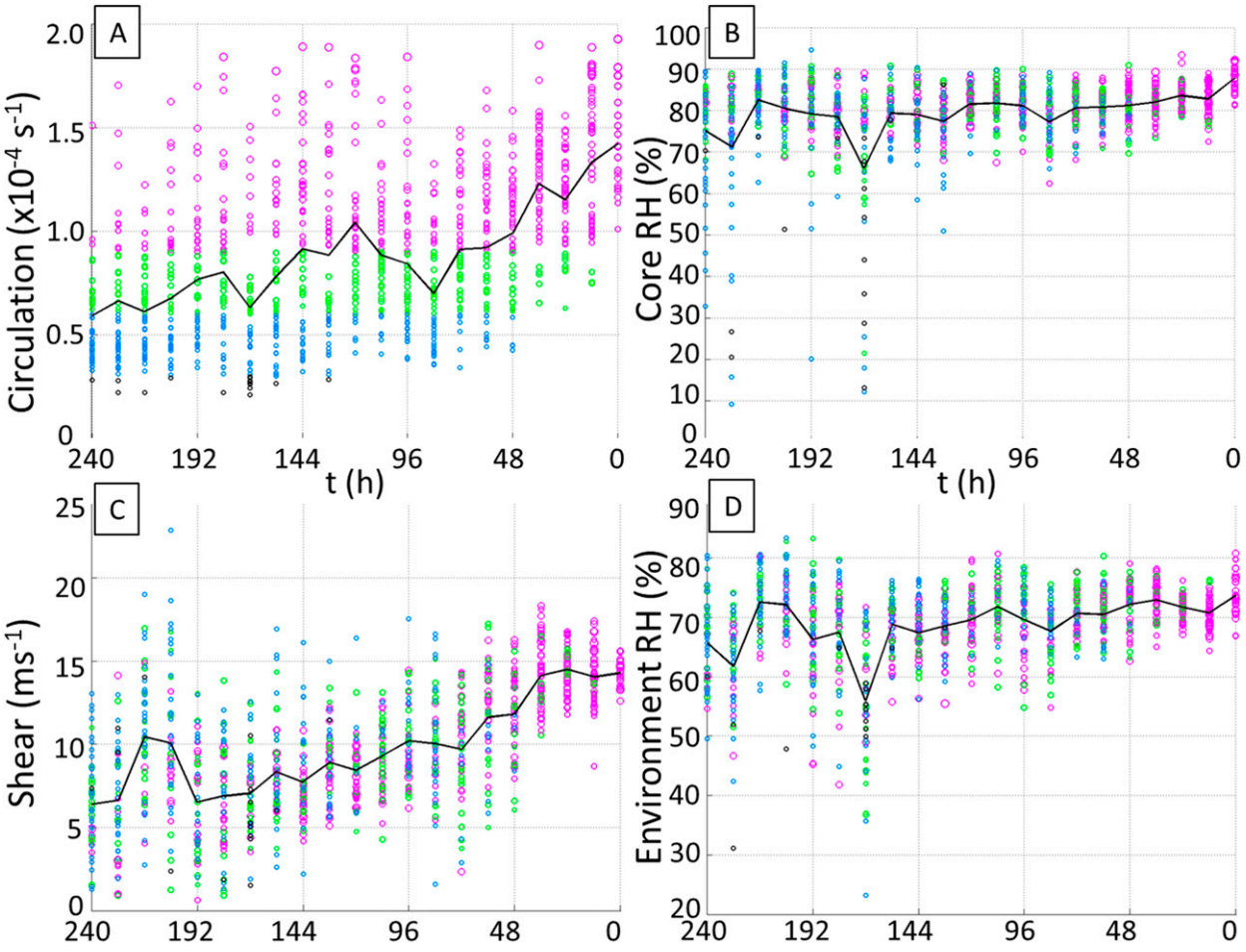

FIG. 5. As in Fig. 2, but for the genesis of Hurricane Igor. Forecasts are valid at 1200 UTC 8 Sep 2010.

times, better agreement for a strong wave exiting the coast of western Africa resulted in a very strong genesis signal. Igor was also associated with not only a very moist core (Fig. 5b), but also a very moist surrounding environment (Fig. 5d). In fact, Igor developed in the moistest environment at 700 hPa of all the systems in 2010. Igor demonstrates that a very moist environment can help a wave overcome other challenges during development, such as high shear. Unlike Fiona and Earl, the individual ensemble members with the strongest circulations were not necessarily associated with lower shear or higher core moisture.

Another noteworthy aspect of Igor was the fact that the circulation forecasts valid at the genesis time were associated with unusually high variance even at very short lead times (Fig. 5a). While there was low uncertainty in the forecast for moisture (Fig. 5b) due to a combination of low ensemble variance and a lack of any sharp moisture gradients near the center of circulation in any ensemble member (Fig. 6a), there was considerable uncertainty even at short lead times in the strength of the shear (Fig. 5c). This was due to the fact that the wave associated with Igor was traversing through a very sharp gradient in shear and a local maximum in forecast variance of shear, evident in forecasts from 36-h lead time (Fig. 6b). So while Igor managed to develop in a seemingly unfavorable environment with higher values of shear, it nonetheless appears that uncertainty in the strength of the shear still translated to uncertainty in the strength of circulation.

d. Bonnie

The predictability of the genesis of Bonnie is particularly difficult to relate to changes in its environment. Although in many other cases the ensemble distribution shifts from weak to strong circulations at a time when the environment is forecast to become more favorable, an increase in the predicted circulation from 72–96-h lead time (Fig. 7a) occurs with seemingly no major changes in predicted moisture or shear (Figs. 7b,c). Not only were the changes with time in predicted moisture and shear fairly insignificant, but the actual verifying values were not

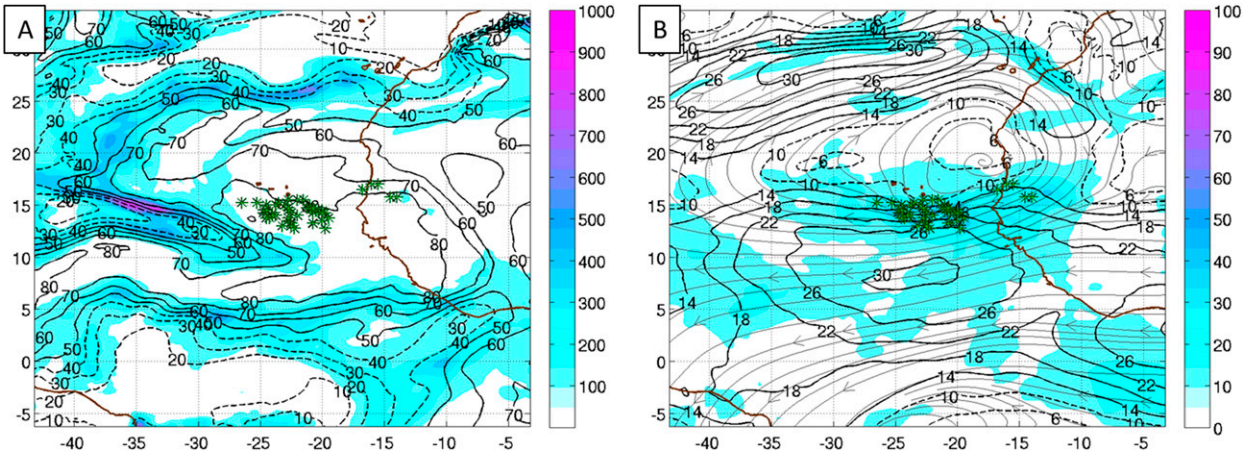

FIG. 6. The predicted location of Igor at the time of genesis relative to (a) gradients of moisture and (b) gradients of shear in 36-h forecasts initialized at 0000 UTC 7 Sep 2010. Included are (a) ensemble mean RH at 700 hPa (contours) and forecast variance for RH (color shaded), and (b) ensemble mean 850–200-hPa shear (black contours), ensemble mean streamlines of 850–200-hPa shear (gray streamlines), and variance of shear (color shaded). The center of circulation in each ensemble member is indicated (asterisks).

particularly noteworthy either. The core and environment were slightly drier than the 2010 average at 82% and 58%, respectively, but well within the variance of the sample. Shear was also neither unusually high nor low at 6 m s^{-1}. The strength of the predicted divergence appears to be correlated to the strength of the disturbance at the same forecast time (Fig. 7d). However, this is not necessarily the cause for a stronger genesis signal and can often be attributed as an effect of having a stronger initial vortex at shorter lead times.

Also interesting is the time variation of the change in spread of circulation forecasts for Bonnie (Fig. 7a). At early lead times (240–108 h), the spread is low and the ensemble is completely underdispersive. Here the initial vortex is too weak in all the members and almost universally fails to develop. At later lead times (96–48 h), some members have a stronger initial vortex but with large forecast uncertainty, leading to a high variance forecast. Finally, at shorter lead times (36–0 h), the entire ensemble initializes a stronger vortex but with lower forecast uncertainty, thereby once again producing a lower spread forecast.

Another attribute of Bonnie was the fact that it originated from an anomalously small wave, especially for 2010. It is likely that its small size made Bonnie difficult for the ensemble to accurately predict more than 72 h before genesis, likely due to a combination of sampling and resolution issues. It is apparent by $t = 36$ h that the forecast initialized at 0000 UTC 19 July 2010 (Fig. 8a) will only result in a modest circulation by $t = 84$ h (Fig. 8b) at the verifying time of genesis. However, many ensemble members initialized just 12 h later on 19 July 2010 already depict a much stronger wave at $t = 24$ h (Fig. 8c), which ultimately yields a much stronger genesis likelihood by $t = 72$ h (Fig. 8d). So while many genesis events in 2010 showed considerable sensitivity to the environment, the dominant sensitivity for Bonnie appears to be to the strength of the initial circulation. Bonnie exemplifies the difficulty that global model ensembles often have with initializing weak waves accurately.

e. *Remaining cases*

In several cases similar to Earl, a clear relationship was found to exist between ensemble members with the highest moisture and/or lowest shear and the strength of the predicted circulation (Alex, Colin, Danielle, Gaston, Hermine, Matthew, Otto, Shary, and Tomas). Also for these cases, forecasts with greater variance in moisture or shear were generally associated with greater variance in the predicted strength of circulation. For other cases (Tropical Depression 2, Tropical Depression 5, Julia, Karl, Lisa, Nicole, Paula, and Richard), there was not a clear relationship between the favorability of the environment and the strength of circulation in individual forecasts. Note that there is no clear distinction between easterly wave and non-easterly wave genesis events, similar to the findings of Majumdar and Torn (2014).

In a few of the cases in which the predictability of genesis cannot be easily related to the environment, there existed a stronger relationship between the strength of the initial vortex and the strength of the verifying circulation. Examples include Bonnie, Lisa, and Igor. In only the case of Nicole, the forecast strength of circulation at the time of genesis was strongly dependent upon the location, not strength, of the initial vortex prior to genesis. Finally, for Fiona and Lisa, there was virtually no genesis signal in forecasts initialized while the easterly waves

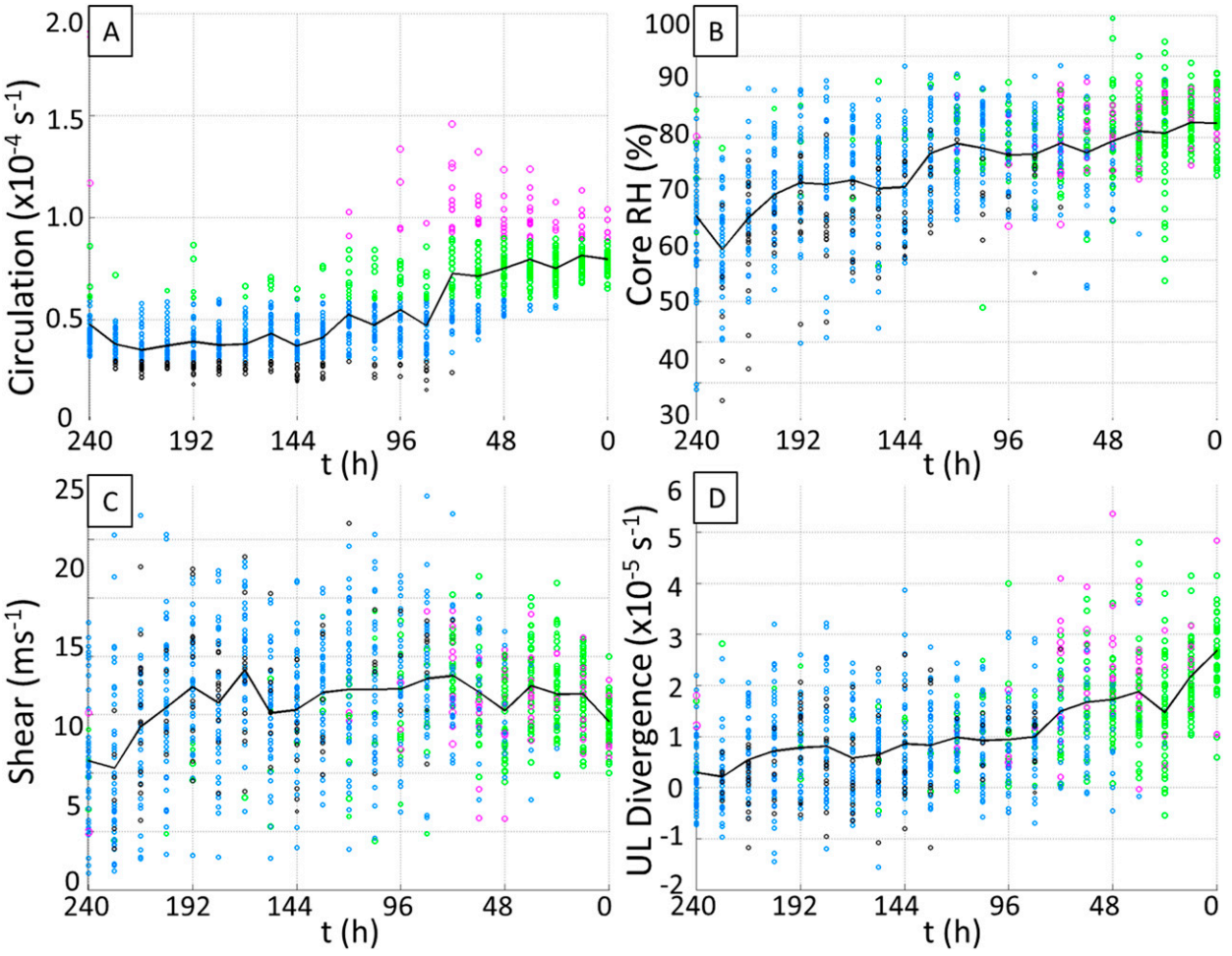

FIG. 7. As in Fig. 4, but for time of genesis (1200 UTC 22 Jul 2010) for Tropical Storm Bonnie and (d) core 200-hPa divergence (s^{-1}).

were still located over Africa. Thereafter, all subsequent forecasts resulted in a strong genesis signal within a day of the wave emerging over water from the West African coast. Last, the pattern of decreased (enhanced) predictability when genesis occurs near (away from) sharp gradients in moisture and/or shear described in the case of Earl is also observed in a few other genesis events.

4. Joint distributions

The joint distributions in this section represent composites of the relationships between variables in all 51 ensemble members, cumulative over all 21 genesis events. Unless otherwise stated, forecasts over the entire 0–240-h time frame are included.

We begin our exploration of the multivariate phase space of variables relevant to genesis by examining the relationship between moisture and strength of circulation. The joint distribution for 700-hPa core RH and circulation reveals the expected result of an increase in the number of cases with strong circulations given higher values of moisture (Fig. 9a). While higher moisture does not necessarily preclude the existence of weaker circulation, as there are still a few counts in the bins of high RH/low circulation, it appears that core RH $< 60\%$ almost certainly prevents circulation from reaching $1 \times 10^{-4}\,s^{-1}$. The sample also appears to be heavily biased toward cases with core RH between 70% and 90%. There are very few samples of low RH since only those cases in which genesis actually occurs are included. On the other hand, there are very few cases exceeding 90% RH simply because it is very difficult to sustain such a high moisture content over a region 600 km in diameter. Therefore, to account for unequal samples within each RH bin, each column is normalized by the total number of cases contained within it (Fig. 9b). Doing so gives a clear depiction that the higher the RH, the greater the potential for a system to have a stronger circulation, due to an increased fraction of that column being associated with stronger circulation values. Similarly, if RH is $<60\%$, it is

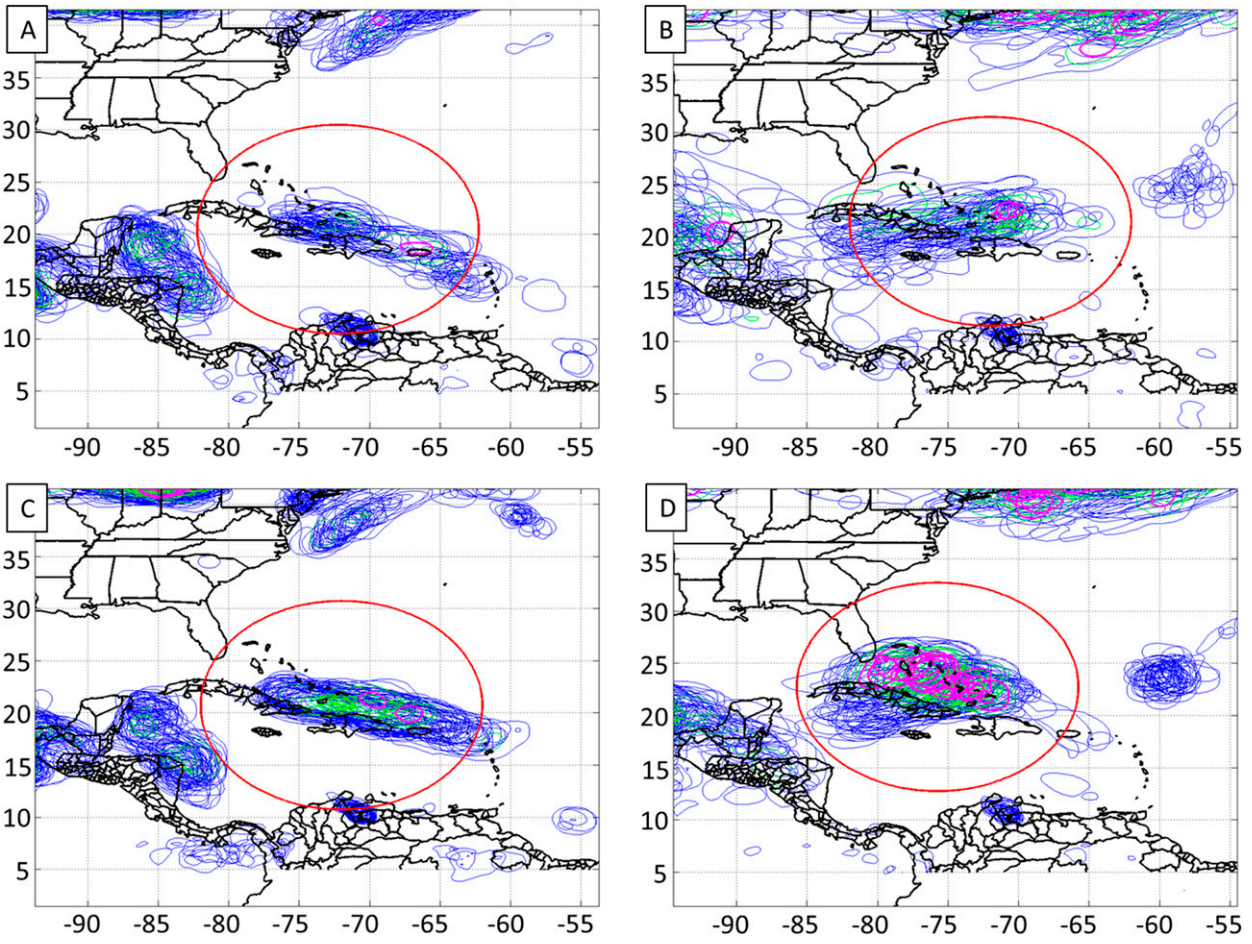

FIG. 8. Composite circulation forecasts for all ensemble members valid (a),(c) 48 h prior to the genesis of Bonnie and (b),(d) at the time of genesis of Bonnie contoured in $3 \times 10^{-5}\,s^{-1}$ (blue), $6 \times 10^{-5}\,s^{-1}$ (green), and $9 \times 10^{-5}\,s^{-1}$ (magenta) increments. Included are (a) a 36-h forecast and (b) an 84-h forecast initialized at 0000 UTC 19 Jul 2010, and (c) a 24-h forecast and (d) a 72-h forecast initialized at 1200 UTC 19 Jul 2010.

most likely that the circulation of the wave will fall between 2.5 and $5.0 \times 10^{-5}\,s^{-1}$.

The joint distribution of forecast *errors* for circulation and 700-hPa core RH (Fig. 9c), where we now subtract verification from each case, depict an overall similar structure to the joint distribution of the variables themselves (Fig. 9a). Additionally, the dry bias is revealed in the error computation, and cases with this bias are also associated with a weak circulation bias. It is not surprising that there are many more cases with dry errors than moist errors, since only cases in which genesis actually occurred are included in our sample. With a sample of cases in which verification for RH is consistently in the 80%–90% range, it is physically impossible to obtain errors much greater than +20%, but it is not difficult to have errors of −40%.

In contrast to the clear relationship between the circulation and core RH in Fig. 9b, a relationship between the environmental RH ($300 \le r \le 1000$ km) and circulation is much less obvious, even with normalization (Fig. 9d). While RH less than 30% appears to be a hard cutoff for nondevelopment, its sample size is quite low. However, values as low as 30%–40% RH appears to be almost as favorable as 80%–90% RH.

An examination of the joint distribution between circulation and core RH for different subsets of lead times reveals that a dry bias has already appeared in 0–72-h forecasts, suggesting a possible problem in the model physics or parameterizations (Fig. 10a). Thereafter, the dry bias becomes progressively stronger with increasing lead times (Figs. 10b,c). There is also a weak bias for circulation that grows with lead time. While this weak bias is again related to the dry bias, the fact that the sample only includes developing systems is also a likely contributor.

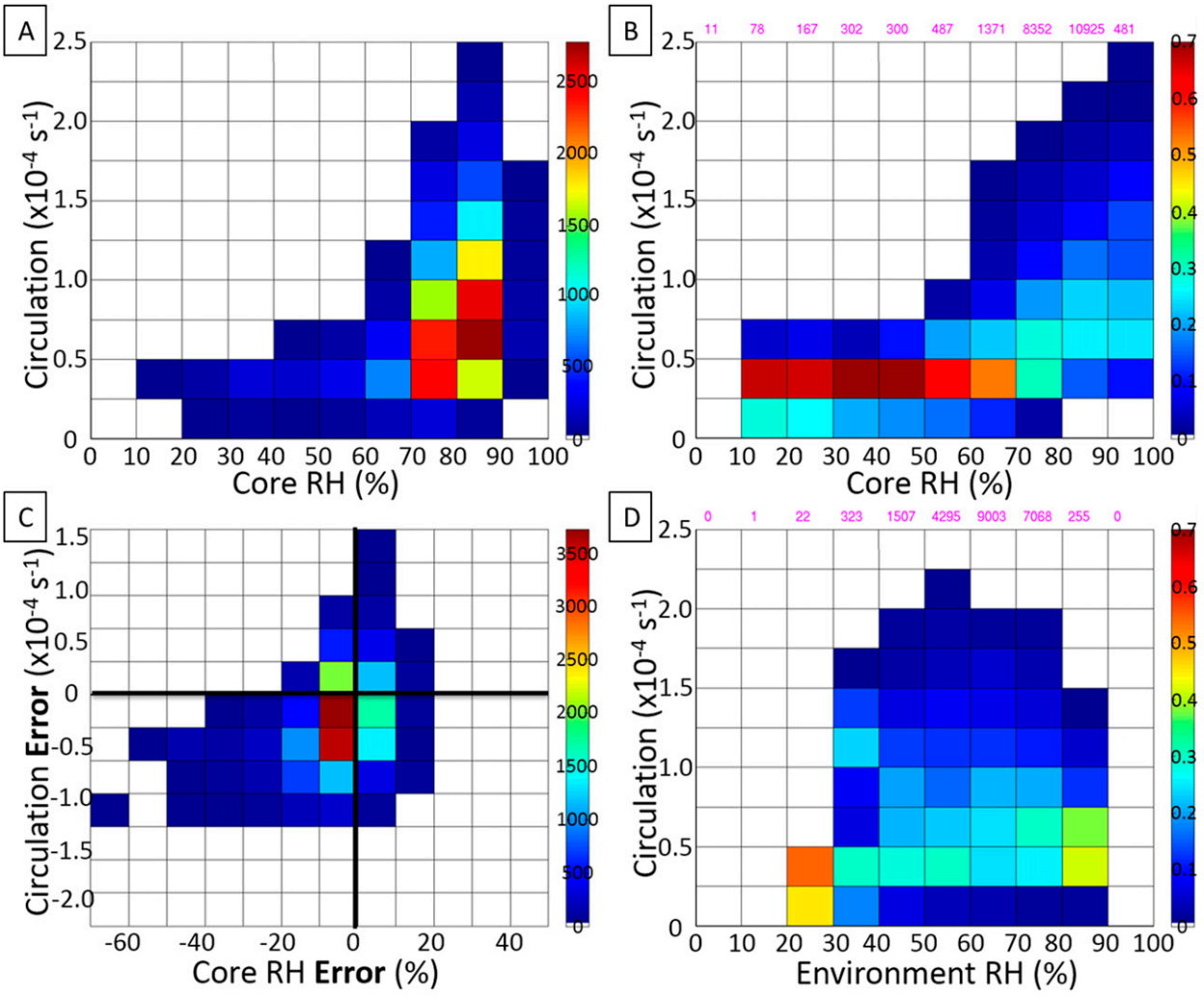

FIG. 9. (a) Joint distribution, (b) normalized joint distribution, and (c) error distribution of circulation vs 700-hPa core RH; (d) normalized joint distribution of circulation vs 700-hPa environmental RH. In (b) and (d), the total number of elements in each column is labeled at the top (magenta).

A relationship between circulation and latitude has been suggested in the case study of Earl (section 3a). The corresponding joint distribution over the 2010 season reveals that the stronger circulations do exist at higher latitudes (Fig. 11a). However, this is likely just an artifact of a stronger β effect for stronger circulations, demonstrated in Fiorino and Elsberry (1989). To calculate the effect of circulation on deep-layer mean steering flow, an average of the 5-day forecast 850–500-hPa meridional winds within a $1000 \times 1000\,\text{km}^2$ box for all 21 tropical waves is computed, with the difference between the 5 strongest and the 5 weakest ensemble members computed for each case. Overall, the meridional component of wind is found to be $1.00\,\text{m s}^{-1}$ stronger (and southerly) for the five strongest ensemble members than for the five weakest members. Linearly extrapolated for an additional 120 h, this would translate to a latitudinal difference of 432 km. Therefore, the tropical wave gains more latitude in ensemble members with stronger circulations, consistent with Fig. 11a. Also consistent with Figs. 11a and 9d, a negative relationship between latitude and environmental RH is revealed in Fig. 11b.

Joint distributions can sometimes be more complex than the preceding cases. One example is the distribution of core RH versus environmental RH (Fig. 11c). While the distribution exhibits a clear maximum in the 60%–80% environmental RH and 70%–90% core RH bins, there are two local maxima in the core RH distribution for low environmental RH in the 30%–50% range. An examination of the three-dimensional joint distribution between core RH, environmental RH, and

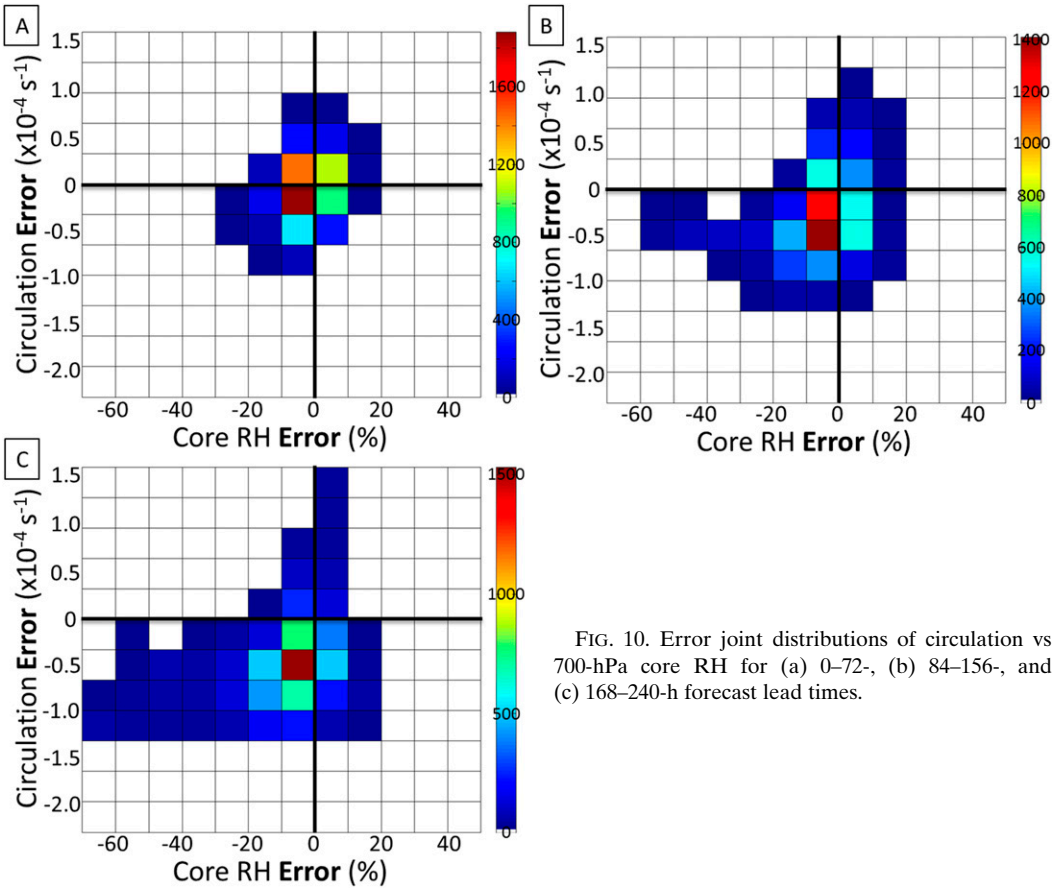

FIG. 10. Error joint distributions of circulation vs 700-hPa core RH for (a) 0–72-, (b) 84–156-, and (c) 168–240-h forecast lead times.

circulation in Fig. 11d first reveals that the dry environment/dry core cases are associated with weak circulations. On the other hand, dry environment/moist core cases are associated with strong circulations (red circle), likely due to stronger circulations recurving northward more rapidly into dry midlatitude air and/or the Saharan air layer due to increased β advection. These dry environment/moist core cases can largely be attributed to waves such as Fiona and Earl, in which a localized region of higher RH becomes detached from a moist environment to the south and/or east but remains collocated with the circulation maximum (Fig. 3). In the absence of hostile shear or significant dry air penetrating the core, the system remains resistant to the relatively dry environment and ultimately undergoes genesis.

As expected, stronger circulations are associated with stronger upper-level divergence (Fig. 12a). A nonnegligible number of developing cases do feature net low-level divergence. However, the presence of net low-level divergence >48 h prior to genesis is not inconsistent with observations (e.g., Bister and Emanuel 1997; Komaromi 2013), during which time downdrafts often still dominate over any developing secondary circulation. In addition to some of these cases being nondevelopers, there also appear to be a significant fraction of cases featuring low-level divergence in which the dynamics are properly represented, but genesis is simply too slow to occur. On the other hand, there are also a large number of cases that feature net upper-level convergence (Fig. 12b). These forecasts are overwhelmingly nondevelopers, as subsidence suppresses convective activity within the wave.

Divergence at 200 hPa also exhibits a clear positive correlation with 700-hPa RH (Fig. 12c). The more moist the core of the system, the stronger the upper-level divergence can potentially be. Errors in RH and divergence depict a similar relationship (Fig. 12d); a general dry bias in the forecast is associated with a weak bias in the area-averaged divergence. This relationship is likely tied to the strength of the convection and strength of the secondary circulation, either of which are weakened by downdrafts caused by evaporation triggered by dry air. However, it is unclear if the presence of lower RH air necessarily leads to weaker upper-level divergence, or if this distribution also includes cases of weak upper-level divergence resulting in weaker updrafts and less convection, which appears as lower RH air at 700 hPa.

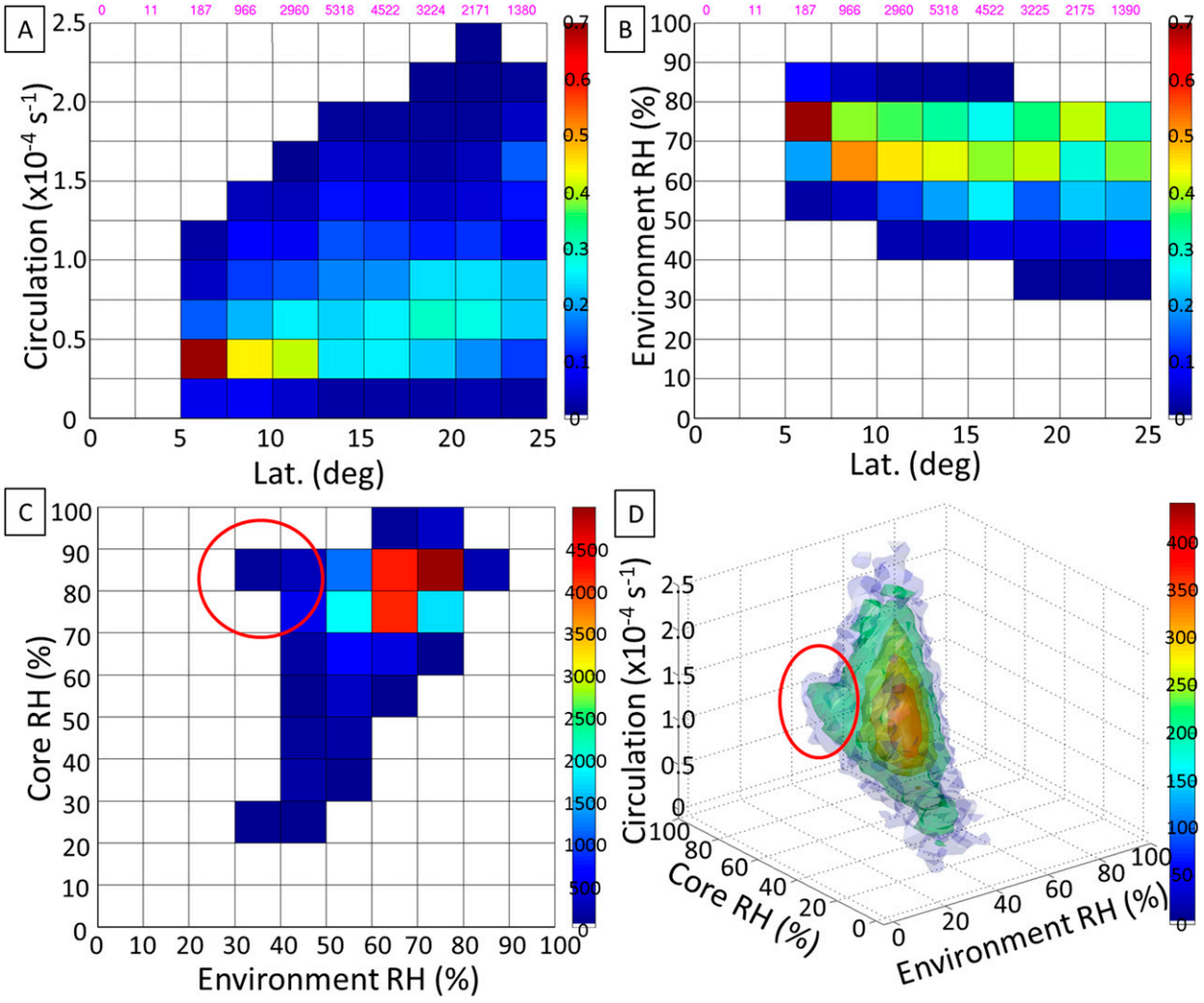

FIG. 11. (a) Normalized joint distribution of circulation vs latitude, (b) normalized joint distribution of 700-hPa environmental RH vs latitude, (c) joint distribution of 700-hPa core RH vs 700-hPa environmental RH, and (d) three-dimensional joint distribution of 700-hPa core RH, 700-hPa environmental RH, and circulation. In (a) and (b), the total number of elements in each column is labeled at the top (magenta).

Next, relationships that involve vertical wind shear are examined. Normalized distributions of 850–200 (Fig. 13a) and 850–500 hPa (not shown) wind shear indicate definite trends of stronger circulations for weaker values of shear. However, there is no definitive cutoff for shear above which a circulation $>1.0 \times 10^{-4}\,s^{-1}$ does not occur, as there was for moisture. Also note that for 850–200-hPa shear, 0–2.5 m s^{-1} is virtually identical to 7.5–10 m s^{-1} in terms of favorability for genesis. For comparison, Nolan and McGauley (2012) found that 2.5–3.75 m s^{-1} shear is this most favorable condition, while 0 m s^{-1} shear was about as favorable as 7.5 m s^{-1} shear.

The effects of the zonal component of wind shear are also investigated. The distribution in Fig. 13b suggests that that the zonal shear direction is unrelated to genesis. This contradicts the results of Nolan and McGauley (2012), who found westerly shear to be more favorable. However, environments with westerly shear in this sample are drier (Fig. 13c) and have stronger total shear (Fig. 13d), which are factors known to inhibit genesis. Accounting for these factors, it is possible that there is a causal relationship between zonal shear direction and genesis here. Further analysis could also determine whether the relationship between shear direction and intensification is being obfuscated by other variables [e.g., moisture, by examining part correlations following Sippel et al. (2011)]. However, this is presently beyond the scope of this study.

Finally, normalized lagged distributions for circulation and core moisture depict some signal for causality.

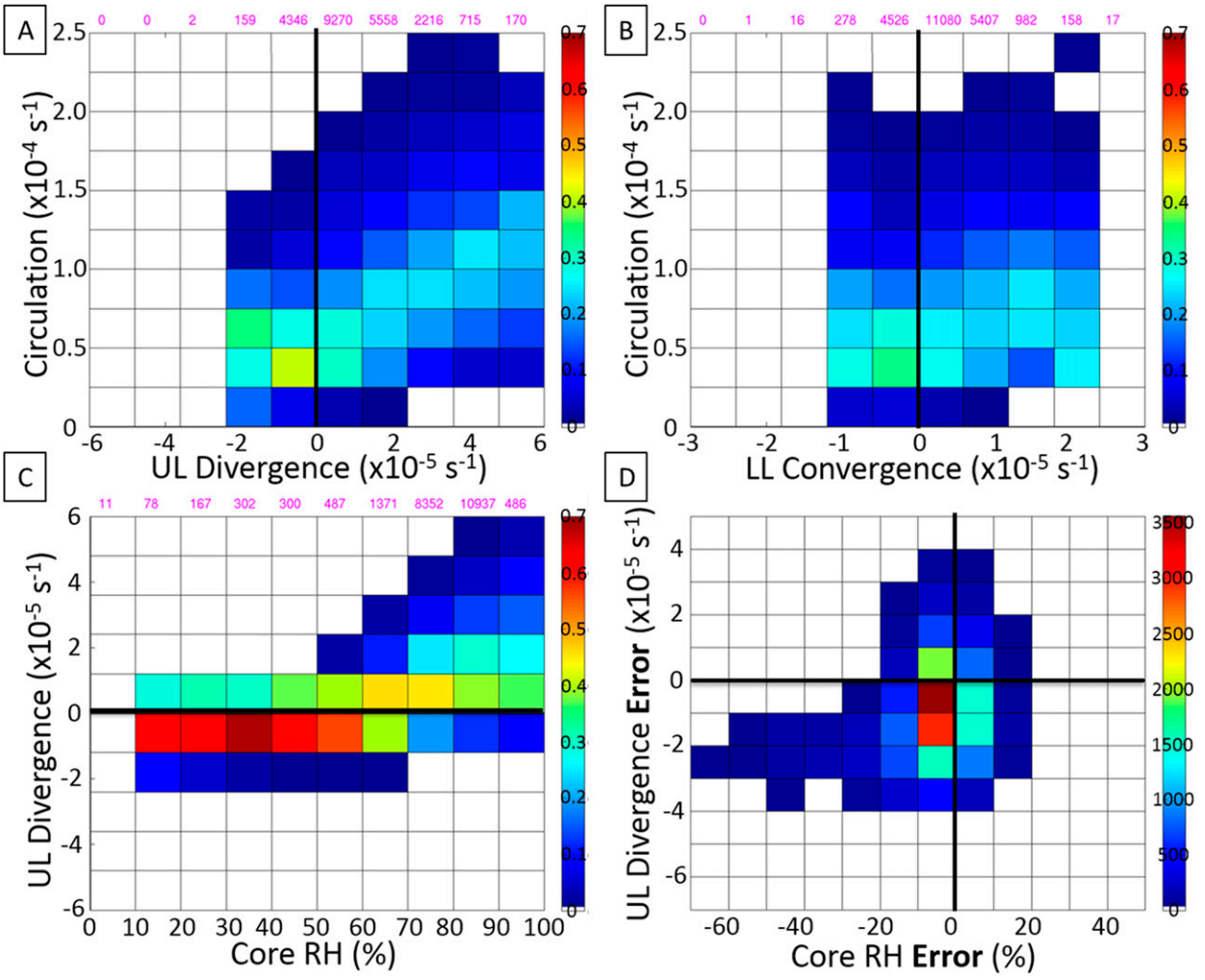

FIG. 12. As in Fig. 11, but for circulation vs (a) 200-hPa core divergence and (b) 850-hPa core convergence; (c) normalized joint distribution of 200-hPa core divergence and 700-hPa core RH; (d) error distribution of 200-hPa core divergence vs 700-hPa error.

While the goal of exploring how one variable affects another at a later time is philosophically similar to performing an ensemble sensitivity analysis (e.g., Doyle et al. 2012), the two techniques differ substantially. Here we have the advantage of not needing a tangent linear model or making any assumptions about linear perturbation growth, but with the disadvantage that it is more difficult to separate the contributions from the individual variables we are assessing. Results indicate that strength of circulation at the time of genesis exhibits a positive relationship with magnitude of the 700-hPa core RH 48 h prior to genesis (Fig. 14a). Conversely, the relationship between core RH at the time of genesis and strength of circulation 48 h prior to genesis is not as evident (Fig. 14b). Therefore, it appears that the presence of a moist core contributes to a stronger genesis signal more so than a strong initial vortex results in a moist core at the time of genesis. Similar methodology applied to core RH and core upper-level divergence does not produce as clear a result. It appears that the degree to which a moist core 48 h prior to genesis contributes to stronger upper-level divergence at the time of genesis (Fig. 14c) is roughly equal to the degree to which stronger upper-level divergence 48 h prior to genesis contributes to a moist core at the time of genesis (Fig. 14d).

5. Wave-relative uncertainty prediction

In this section, one goal is to determine whether the ensemble has greater difficulty conveying uncertainty via ensemble variance in the core of the tropical wave than it does in the nearby environment. Another goal is to examine the change (deterioration) in variance prediction with increasing forecast times.

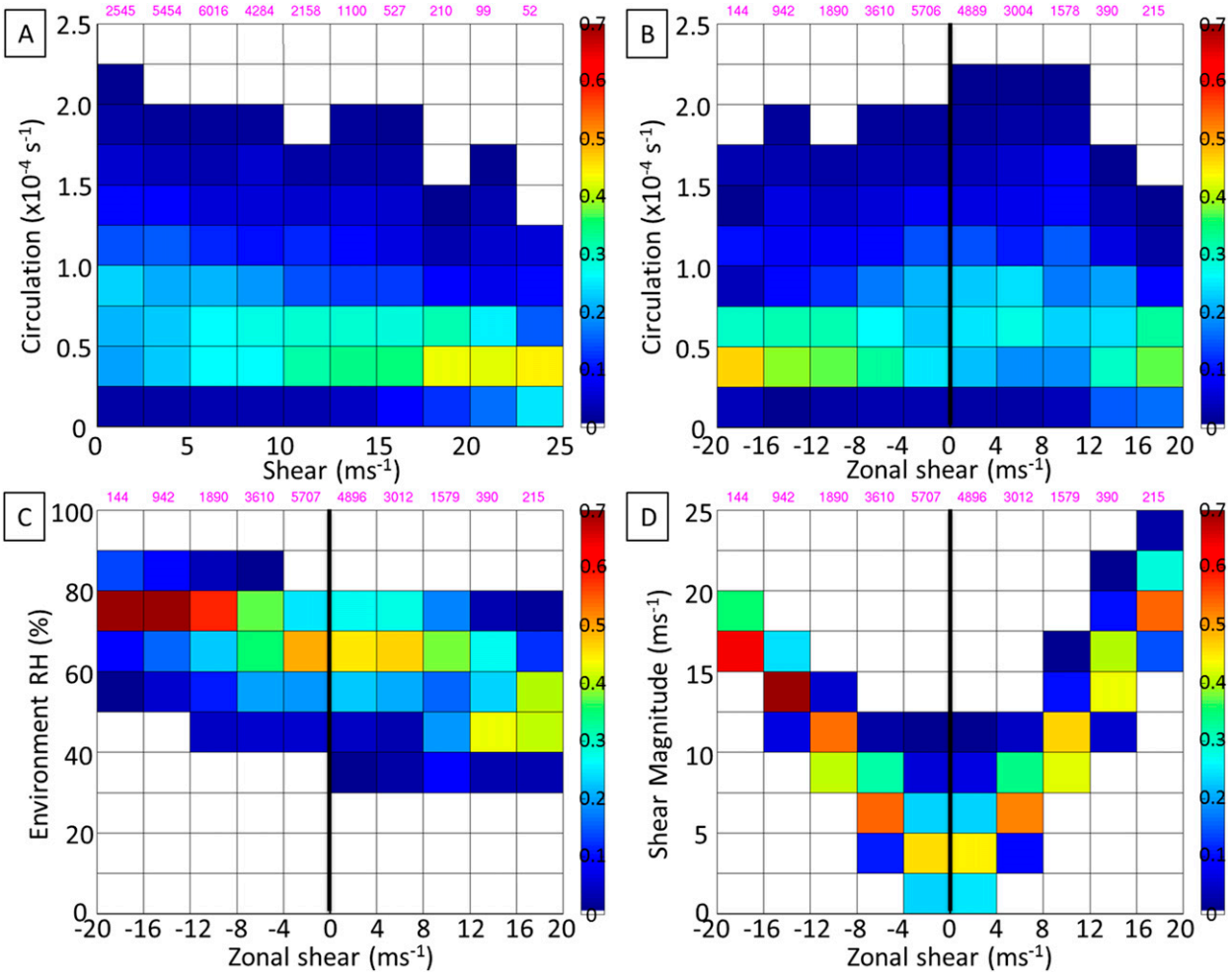

FIG. 13. As in Fig. 11, but for (a) circulation vs 850–200-hPa shear, (b) circulation vs 850–200-hPa zonal shear, (c) 700-hPa environmental RH vs 850–200-hPa zonal shear, and (d) 850–200-hPa shear magnitude vs 850–200-hPa zonal shear.

First, variance prediction for circulation is examined.[1] In general, forecasts with shorter lead times are associated with lower ensemble standard deviation and verify with lower absolute error of the ensemble mean (Fig. 15a, blue dots). While there is too much scatter for a linear regression line to be meaningful, there is nonetheless a positive relationship between the two. Only a few cases fall within the category of poor ensemble performance, where low standard deviation and high error exist, and the lead time in these cases is 6 or more days (Fig. 15a, red dots). A further examination reveals that virtually all of these cases are associated with missed genesis forecasts, in which there is strong agreement within the ensemble that genesis will not occur, but it does (consistent with the findings of Majumdar and Torn 2014). This region of Fig. 15a could also correspond to cases where there is very good agreement that genesis will occur, but it fails to do so, *if* false alarms were included in the sample.

A general increasing relationship between the ensemble-mean error standard deviation and the error of the ensemble mean is found for all lead times (Figs. 15b–d). However, the slope tends to be shallower than the desired 1-to-1 relationship (dashed line), particularly at longer (168–240 h) lead times. In other words, the ensemble mean error is on average too low for high-spread circulation forecasts and is slightly too high for low-spread circulation forecasts. This flattening of the forecast error standard deviation with time is indicative of a model bias, likely the result of a weak bias at longer lead times. If the ensemble is well constructed *and* unbiased, 68% or 1 confidence interval of the sample (dark magenta dots) should fall within the ''ideal'' confidence interval (light magenta cone).

[1] Only core circulation is computed, as environmental circulation is often close to zero.

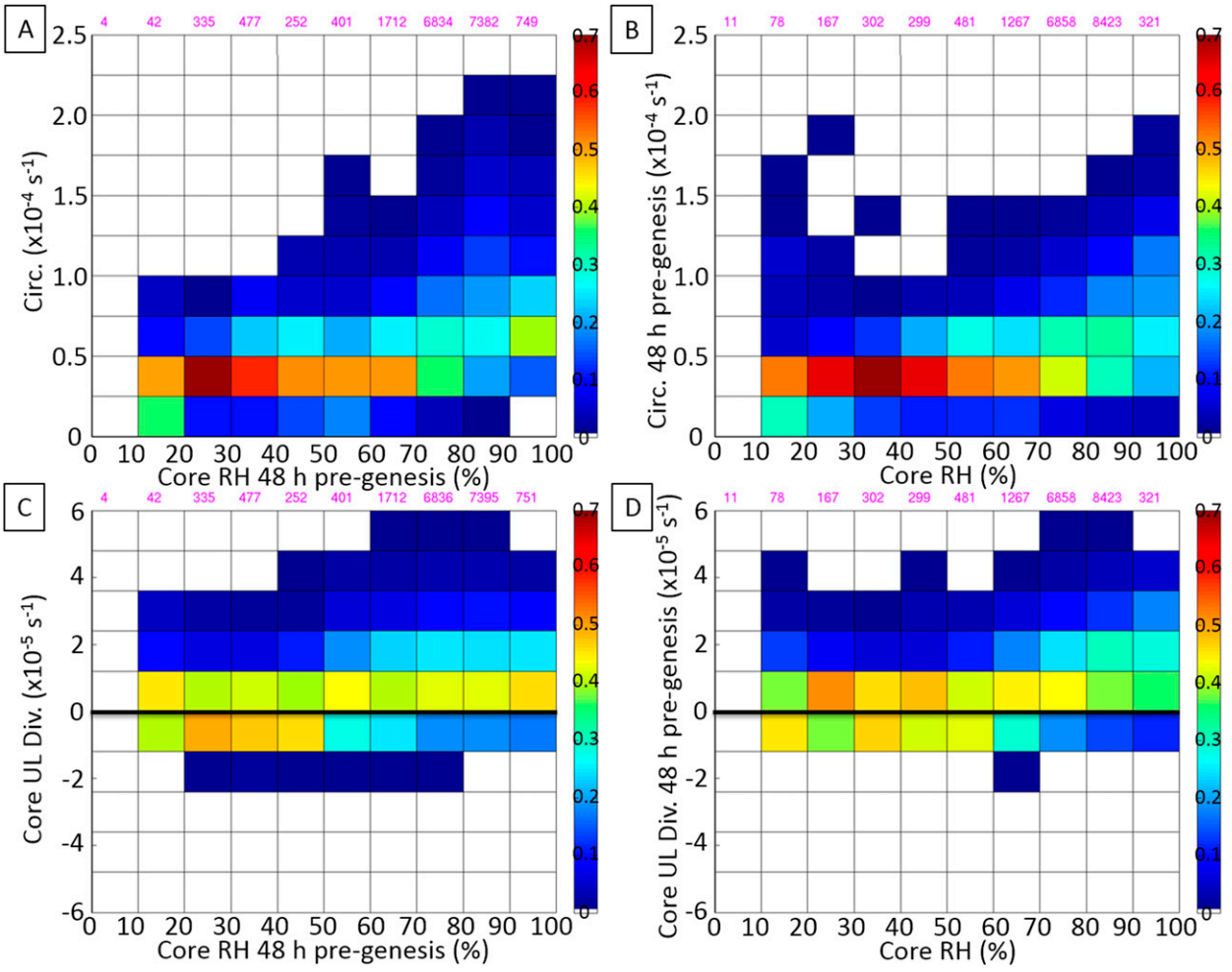

FIG. 14. Normalized lagged distributions: (a) circulation at the time of genesis vs 700-hPa core RH 48 h prior to genesis, (b) circulation 48 h prior to genesis vs 700-hPa core RH at the time of genesis, (c) 200-hPa divergence at the time of genesis vs 700-hPa core RH 48 h prior to genesis, and (d) 200-hPa divergence 48 h prior to genesis vs 700-hPa core RH at the time of genesis. The total number of elements in each column is labeled (magenta).

Many of the magenta dots fall below the ideal distribution at later lead times and with incorrect variance (too much variance for low-error cases, too little variance for high-error cases), indicating that the ensemble forecast bias has become large at +7 days.

The standard deviation and absolute error for core RH exhibits an overall positive relationship, with no cases where the ensemble is dramatically underpredicting the standard deviation (Fig. 16a). The relationship between ensemble mean standard deviation and ensemble-mean error standard deviation also increases for core RH for both 0–72- and 84–156-h lead times (Figs. 16b,c). Higher-variance forecasts of core moisture tend to be associated, on average, with higher error forecasts, implying that the ensemble is adequately conveying the uncertainty in the forecast. However, the relationship begins to fail at 168–240 h, at which time the slope is much shallower than 1:1, implying that forecasts with higher forecast variance are only slightly more likely to verify with higher mean error than forecasts with low variance, thus indicating a dry bias (Fig. 16d). This differs with the results from Part I, where the relationship for 700-hPa RH was still monotonically increasing at 168–240 h on the large scale.

Predictability for 700-hPa RH appears to be slightly greater overall when averaging over the wave environment (Fig. 17), with forecasts noticeably less dry biased at longer lead times (168–240 h). However, the relationship between ensemble mean standard deviation and ensemble-mean error standard deviation does still begin to deviate from a monotonic increase at longer lead times. This demonstrates that the ensemble has greater skill in predicting moisture variance in the environment surrounding these tropical waves than it does

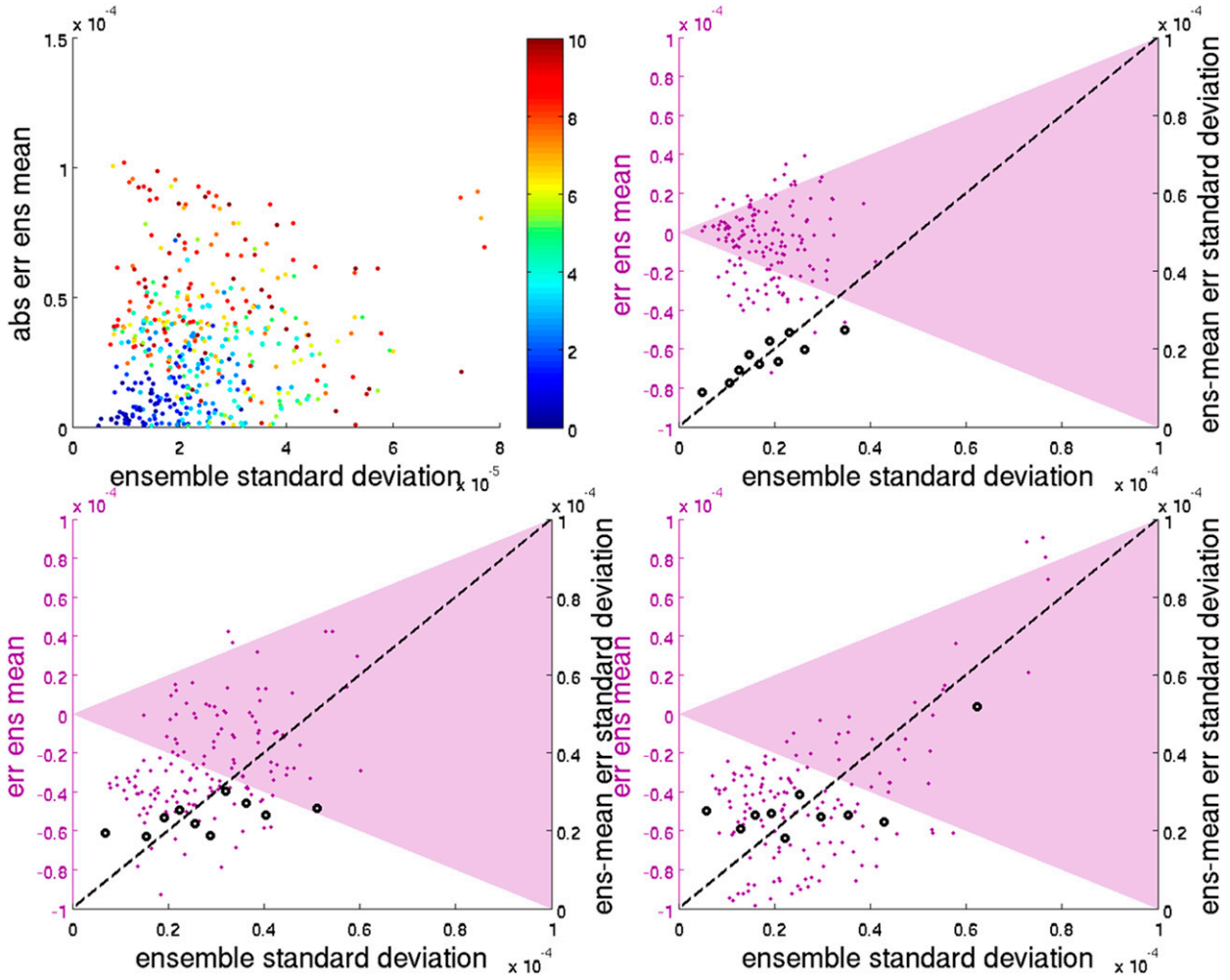

FIG. 15. Evaluation of ensemble variance prediction for wave-relative circulation forecasts. (a) Standard deviation of ensemble forecasts vs the absolute error of the ensemble mean forecast as a function of forecast lead time, in days (colored).(b)–(d) Ensemble standard deviation vs error of the ensemble mean forecast (magenta dots), first confidence interval of the ideal distribution of the sample (magenta cone). Ensemble-mean forecast error standard deviations in 10 equal-sized bins (black circles), and the 1:1 line (dashed) for 0–72, 84–156, and 168–240 h, respectively.

with the moisture local to the waves themselves, but it still has difficulty in the environment beyond 156 h.

While results for shear and divergence are not shown, the general result of the slightly greater ability of the ensemble to predict variance over the environment than over the wave core is still evident. Also, a weak bias in core divergence is not evident on environmental scales, resulting in a more monotonic increasing relationship at longer lead times.

6. Conclusions

This study builds on the basin-scale examination of predictability associated with genesis in Part I by focusing on relatively small domains in the frame of reference relative to the wave. ECMWF ensemble forecasts out to 10 days were employed over 21 cases of genesis in 2010.

As had been concluded in Part I, predictability depends heavily on the flow regime. Some genesis events were found to be more predictable than others, and the factors that limited predictability for some cases were not consistently inhibiting factors across all cases. In conventional cases such as Earl, there is a clear and consistent relationship between the ensemble distribution of circulation at the time of genesis and the overall favorability of the predicted environmental moisture and shear. In these cases, a strong relationship between predicted circulation and core 700-hPa RH in individual ensemble members was noted, consistent with Doyle et al. (2012). In contrast, other cases including Fiona, Igor, and Bonnie exhibited no clear relationship

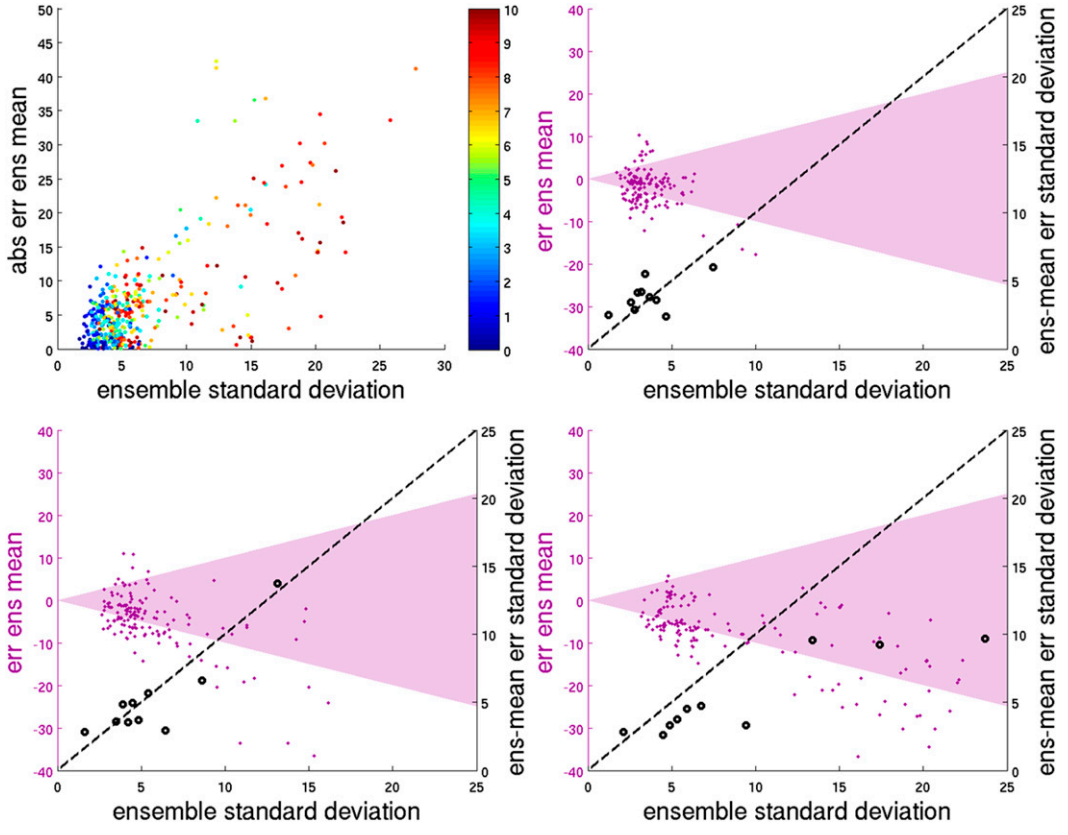

FIG. 16. As in Fig. 15, but for 700-hPa core RH.

between the favorability of the predicted shear and moisture and the circulation. For Bonnie and Igor, a stronger relationship was found between the strength of the initial vortex (or the vortex 48 h prior to time of genesis) and the strength of the circulation. For Fiona (and Lisa; not shown), there was virtually no genesis signal in forecasts initialized while the easterly waves were still located over Africa. Thereafter, all subsequent forecasts resulted in a strong genesis signal within a day of the wave emerging over water from the West African coast. This case-to-case disparity between sensitivity to the initial vortex versus sensitivity to the environment was also found by Sippel et al. (2011) and Torn and Cook (2013).

Despite the case-to-case variability, some general characteristics associated with predictability of genesis were also found. Tropical waves collocated with or traversing sharp gradients in shear or moisture were associated with greater forecast variance and thereby uncertainty for those variables, resulting in greater variance in the predicted strength of circulation. Similarly, tropical waves far from significant gradients tended to be associated with a lower uncertainty environment, which translated to lower variance in the predicted circulation. Another common result was that tropical waves that maintained a moist core while traversing an otherwise sheared or relatively dry environment maintained a consistent genesis signal.

The joint distributions over all the genesis cases revealed a positive correlation between 200-hPa divergence–850-hPa convergence and strength of circulation. However, there were also a nonnegligible number of forecasts associated with net low-level core divergence despite having positive circulation. It is likely that some of these cases are instances where genesis is too slow to occur in the forecast, and the predicted wave was still at the low-level outflow dominant pregenesis stage similar to findings reported by Bister and Emanuel (1997) and Komaromi (2013). Most of the forecasts with net upper-level convergence were nondevelopers.

There was also little to no correlation between environmental moisture and circulation, but a strong positive correlation between core moisture and circulation. Lagged joint distributions revealed that a dry core was more likely to result in a weaker genesis signal than it was to be the result of a weak vortex. The finding that dry air was less detrimental to stronger, more mature circulations is consistent with Sippel et al. (2011). In several cases, most notably Earl and Fiona, the waves appears to resist the intrusion of dry environmental air

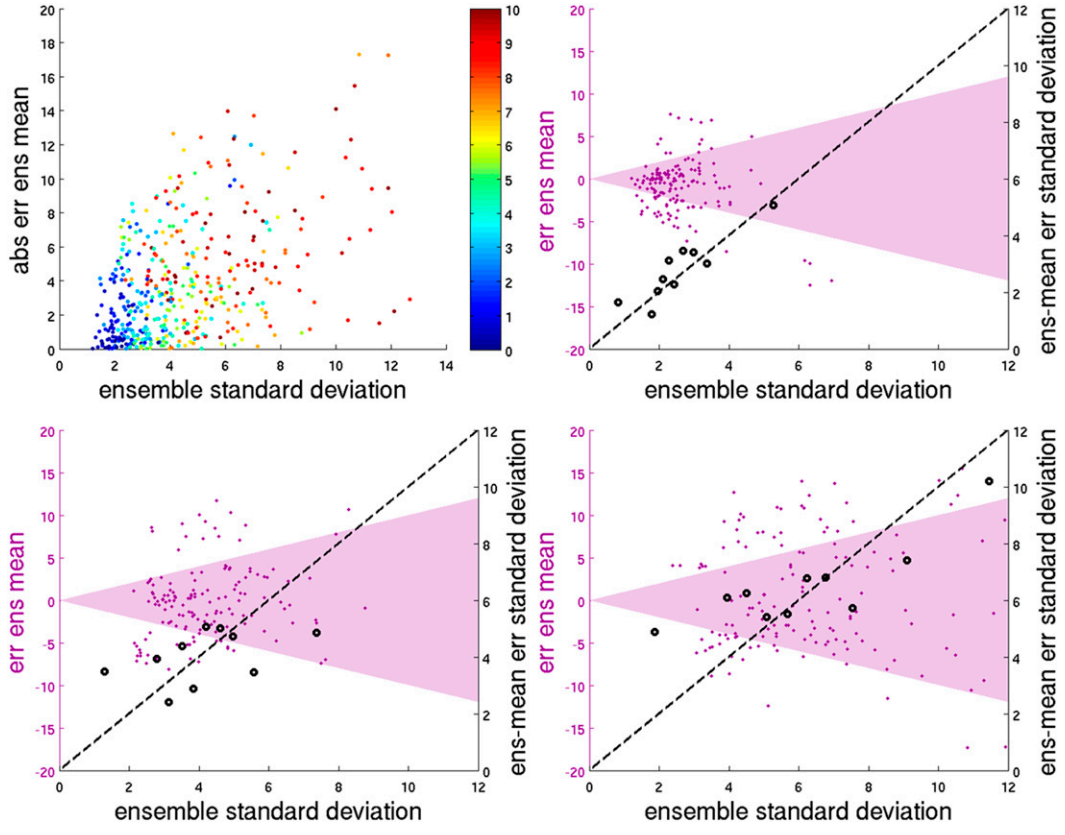

FIG. 17. As in Fig. 15, but for 700-hPa environmental RH.

within the recirculating region, consistent with the findings of Dunkerton et al. (2009) and Braun et al. (2012, 2013). However, none of these waves were in the presence of strong shear. It is also worth noting that the ensemble exhibited a dry bias, which became more pronounced at longer lead times.

Greater values of vertical wind shear were associated with weaker predicted circulation at the time of genesis. However, a few ensemble members did develop stronger circulations with up to 20–25 m s^{-1} deep-layer shear, demonstrating that greater shear values may suppress but not prevent genesis. Neither westerly nor easterly shear were found to be more favorable than the other.

By averaging forecasts over the inner core and an environmental annulus, wave-relative variance prediction was generally superior to the parallel evaluations on synoptic scales in Part I. For all variables examined, the relationship between ensemble standard deviation and ensemble-mean error standard deviation was mostly increasing with a slope near unity. For 7–10-day forecasts, some cases of low ensemble standard deviation and high mean error for circulation existed, which were associated with an underdispersive ensemble. The overall ''flattening'' of the variance–error relationship at longer forecast times was likely due to the growth of model biases, with a dry bias being the most evident.

To conclude, the ECMWF ensemble has demonstrated that, not only are the environmental conditions favorable to genesis predictable out to a week or more, but there is some predictability associated with the individual genesis events themselves out to similar lead times. However, all cases are different, and some genesis events are found to be much more predictable than others. Ultimately, a combination of improved modeling, data assimilation, and increased observations should be able to extend our ability to predict TC genesis even further.

Acknowledgments. The authors gratefully acknowledge funding from the National Research Council, as well as the National Science Foundation (Grant ATM-0848753). The authors thank Rich Rotunno and Chris Davis of NCAR, Ryan Torn of SUNY at Albany, and Brian Mapes and David Nolan of the University of Miami for their comments and suggestions on this study. We would also like to thank Jason Sippel and one anonymous reviewer, whose comments improved this paper. Last, we thank TIGGE for the availability of the data used in this study.

REFERENCES

Bister, M., and K. A. Emanuel, 1997: The genesis of Hurricane Guillermo: TEXMEX analyses and a modeling study. *Mon. Wea. Rev.,* **125,** 2662–2682, doi:10.1175/1520-0493(1997)125<2662:TGOHGT>2.0.CO;2.

Bougeault, P., and Coauthors, 2010: The THORPEX Interactive Grand Global Ensemble. *Bull. Amer. Meteor. Soc.,* **91,** 1059–1072, doi:10.1175/2010BAMS2853.1.

Braun, S. A., J. A. Sippel, and D. S. Nolan, 2012: The impact of dry midlevel air on hurricane intensity in idealized simulations with no mean flow. *J. Atmos. Sci.,* **69,** 236–257, doi:10.1175/JAS-D-10-05007.1.

——, ——, C.-L. Shie, and R. A. Boller, 2013: The evolution and role of the Saharan air layer during Hurricane Helene (2006). *Mon. Wea. Rev.,* **141,** 4269–4295, doi:10.1175/MWR-D-13-00045.1.

DelSole, T., 2004: Predictability and information theory. Part I: Measures of predictability. *J. Atmos. Sci.,* **61,** 2425–2440, doi:10.1175/1520-0469(2004)061<2425:PAITPI>2.0.CO;2.

Doyle, J. D., C. A. Reynolds, C. Amerault, and J. Moskaitis, 2012: Adjoint sensitivity and predictability of tropical cyclogenesis. *J. Atmos. Sci.,* **69,** 3535–3557, doi:10.1175/JAS-D-12-0110.1.

Dunkerton, T. J., M. T. Montgomery, and Z. Wang, 2009: Tropical cyclogenesis in a tropical wave critical layer: Easterly waves. *Atmos. Chem. Phys.,* **9,** 5587–5646, doi:10.5194/acp-9-5587-2009.

Fiorino, M., and R. L. Elsberry, 1989: Some aspects of vortex structure related to tropical cyclone motion. *J. Atmos. Sci.,* **46,** 975–990, doi:10.1175/1520-0469(1989)046<0975:SAOVSR>2.0.CO;2.

Grimit, E. P., and C. F. Mass, 2007: Measuring the ensemble spread–error relationship with a probabilistic approach: Stochastic ensemble results. *Mon. Wea. Rev.,* **135,** 203–221, doi:10.1175/MWR3262.1.

Halperin, D. J., H. E. Fuelberg, R. E. Hart, J. H. Cossuth, P. Sura, and R. J. Pasch, 2013: An evaluation of tropical cyclone genesis forecasts from global numerical models. *Wea. Forecasting,* **28,** 1423–1445, doi:10.1175/WAF-D-13-00008.1.

Komaromi, W. A., 2013: An investigation of composite dropsonde profiles for developing and nondeveloping tropical waves during the 2010 PREDICT field campaign. *J. Atmos. Sci.,* **70,** 542–558, doi:10.1175/JAS-D-12-052.1.

——, and S. J. Majumdar, 2014: Ensemble-based error and predictability metrics associated with tropical cyclogenesis. Part I: Basinwide perspective. *Mon. Wea. Rev.,* **142,** 2879–2898, doi:10.1175/MWR-D-13-00370.1.

Majumdar, S. J., and R. D. Torn, 2014: Probabilistic verification of global and mesoscale ensemble forecasts of tropical cyclogenesis. *Wea. Forecasting,* **29,** 1181–1198, doi:10.1175/WAF-D-14-00028.1.

——, C. H. Bishop, B. J. Etherton, I. Szunyogh, and Z. Toth, 2001: Can an ensemble transform Kalman filter predict the reduction in forecast error variance produced by targeted observations? *Quart. J. Roy. Meteor. Soc.,* **127,** 2803–2820, doi:10.1002/qj.49712757815.

Montgomery, M. T., and Coauthors, 2012: The Pre-Depression Investigation of Cloud Systems in the Tropics (PREDICT) experiment: Scientific basis, new analysis tools, and some first results. *Bull. Amer. Meteor. Soc.,* **93,** 153–172, doi:10.1175/BAMS-D-11-00046.1.

Nolan, D. S., and M. G. McGauley, 2012: Tropical cyclogenesis in wind shear: Climatological relationships and physical processes. *Cyclones: Formation, Triggers, and Control,* K. Oouchi and H. Fudeyasu, Eds., Nova Science Publishers, 1–36.

Poterjoy, J., and F. Zhang, 2014: Predictability and genesis of Hurricane Karl (2010) examined through the EnKF assimilation of field observations collected during PREDICT. *J. Atmos. Sci.,* **71,** 1260–1275, doi:10.1175/JAS-D-13-0291.1.

Schneider, T., and S. M. Griffies, 1999: A conceptual framework for predictability studies. *J. Climate,* **12,** 3133–3155, doi:10.1175/1520-0442(1999)012<3133:ACFFPS>2.0.CO;2.

Sippel, J. A., and F. Zhang, 2008: A probabilistic analysis of the dynamics and predictability of tropical cyclogenesis. *J. Atmos. Sci.,* **65,** 3440–3459, doi:10.1175/2008JAS2597.1.

——, S. A. Bruan, and C.-L. Shie, 2011: Environmental influences on the strength of Tropical Storm Debby (2006). *J. Atmos. Sci.,* **68,** 2557–2581, doi:10.1175/2011JAS3648.1.

Smith, R. K., and M. T. Montgomery, 2012: Observations of the convective environment in developing and non-developing tropical disturbances. *Quart. J. Roy. Meteor. Soc.,* **138,** 1721–1739, doi:10.1002/qj.1910.

Torn, R. D., and D. Cook, 2013: The role of vortex and environment errors in genesis forecasts of Hurricanes Danielle and Karl (2010). *Mon. Wea. Rev.,* **141,** 232–251, doi:10.1175/MWR-D-12-00086.1.

Wang, X., and C. H. Bishop, 2003: A comparison of breeding and ensemble transform Kalman filter ensemble forecast schemes. *J. Atmos. Sci.,* **60,** 1140–1158, doi:10.1175/1520-0469(2003)060<1140:ACOBAE>2.0.CO;2.